Antibacterial, DNA Interaction and Cytotoxic Activities of Pendant-Armed Polyamine Macrocyclic Dinuclear Nickel(II) and Copper(II) Complexes

P. Arthi, A. Haleel, P. Srinivasan, D. Prabhu, C. Arulvasu, A. Kalilur Rahiman

PII: S1386-1425(14)00469-7
DOI: http://dx.doi.org/10.1016/j.saa.2014.03.058
Reference: SAA 11891

To appear in: *Spectrochimica Acta Part A: Molecular and Biomolecular Spectroscopy*

Received Date: 20 January 2014
Revised Date: 1 March 2014
Accepted Date: 20 March 2014

Please cite this article as: P. Arthi, A. Haleel, P. Srinivasan, D. Prabhu, C. Arulvasu, A. Kalilur Rahiman, Antibacterial, DNA Interaction and Cytotoxic Activities of Pendant-Armed Polyamine Macrocyclic Dinuclear Nickel(II) and Copper(II) Complexes, *Spectrochimica Acta Part A: Molecular and Biomolecular Spectroscopy* (2014), doi: http://dx.doi.org/10.1016/j.saa.2014.03.058

ANTIBACTERIAL, DNA INTERACTION AND CYTOTOXIC ACTIVITIES OF PENDANT-ARMED POLYAMINE MACROCYCLIC DINUCLEAR NICKEL(II) AND COPPER(II) COMPLEXES

P. Arthi[a], A. Haleel[a], P. Srinivasan[b], D. Prabhu[c], C. Arulvasu[c], A. Kalilur Rahiman[a,*]

[a]*Post-Graduate and Research Department of Chemistry, The New College (Autonomous), Chennai-600 014, India*

[b]*Department of Bioinformatics, Alagappa University, Karaikudi-630 003, India*

[c]*Department of Zoology, University of Madras, Guindy Maraimalai Campus, Chennai-600 025, India*

Abstract

A series of dinuclear nickel(II) and copper(II) complexes (**1**–**6**) of hexaaza macrocycles of 2,6-diformyl-4-methylphenol with three different benzoyl pendant-arms, 2,2'-benzoyliminodi(ethylamine) trihydrochloride (L), 2,2'-4-nitrobenzoyl iminodi(ethylamine) trihydrochloride (L') and 2,2'-3,5-dinitrobenzoyliminodi(ethylamine) trihydrochloride (L") have been synthesized and characterized by spectral methods. The electrochemical studies of these complexes depict two irreversible one electron reduction processes around E^1_{pc} = −0.62 to –0.76 V and E^2_{pc} = –1.21 to –1.31, and nickel(II) complexes (**1**-**3**) exhibit two irreversible one electron oxidation processes around E^1_{pa} = 1.08 to 1.14 V and E^2_{pa} = 1.71 to 1.74 V. The room temperature magnetic moment values (μ_{eff}, 1.52–1.54 BM) indicate the presence of an antiferromagnetic interaction in the binuclear copper(II) complexes (**4**–**6)** which is also observed from the broad ESR spectra with a g value of 2.14–2.15. The synthesized complexes (**1**–**6**) were screened for their antibacterial activity. The results of DNA interaction studies indicate that the dinuclear complexes can bind to calf thymus DNA by intercalative mode and display efficient cleavage of plasmid DNA. Further, the cytotoxic activity of complexes **2**, **5** and **6** on human liver adenocarcinoma (HepG2) cell line has been examined. Nuclear-chromatin cleavage has also been observed with PI staining and comet assays.

***Keywords**:* Pendant-armed macrocycles; Dinuclear complexes; Antibacterial activity; DNA interaction; Cytotoxicity; Apoptosis.

*Corresponding author: Tel: +91 44 2835 0297; fax: +91 44 2835 2883

E-mail address: akrahmanjkr@gmail.com

1. Introduction

The chemistry of macrocyclic compounds has become a fruitful research area due to the ability of these systems to interact with different substrates, such as metal ions or anionic species [1]. The term "macrocycle" is defined as a cyclic macromolecule or a cyclic compound with nine or more members [2]. Coordination chemists generally define a macrocycle more narrowly as a cyclic molecule with three or more potential donor atoms that can coordinate to a metal center. Cabbiness and Margerum introduced the term "macrocyclic effect" to explain the stability of macrocyclic polyamine when compared to their acyclic analogs [3]. Much effort has now been focused on pendant-arm macrocyclic complexes due to the fact that the ligating groups attached to the macrocyclic backbone can offer additional donor groups to produce important changes in the control of the stability, selectivity, stereochemistry and certain thermodynamic parameters [4, 5] or promote the formation of dinuclear or polynuclear metal complexes with interaction between the metal centers as well as act as host for organic cations with different properties and applications [6]. The following two ways are involved in the process of making pendant-arm macrocyclic complexes: (i) The electrophilic substitution or addition reactions have been used in connecting the functional group with the ring framework (ii) "opened cryptands" can be generated by using analogous functional precursors with variable aromatic dialdehydes in the presence of certain metal ions [7].

In recent years, metal complexes of pendant-arm macrocyclic polyamines are of growing interest for applications in biological and medicinal chemistry, in addition to catalysis. Macrocyclic polyamines bearing pendant-arms can effectively bind specific metals with suitable complexation kinetics and stability while attached to a tumor-targeting vector or peptide. These compounds are used in the radiopharmaceuticals for positron-emission tomography (PET), different phases of biological testing against HIV or antitumor activity and DNA interaction [8–10]. Studies on the interaction of pendant-arm macrocyclic complexes with DNA not only gives information about the reactive modes for protein-DNA interactions and probes of DNA structure but also explains the techniques of molecular biology and drug design [11]. In some cases, the toxicity of macrocyclic polyamines was found to decrease with the increased anti-HIV activity when they are coordinated with bivalent metals like nickel and copper [12]. Based upon these criteria researchers are further involved to exploit their derivatives. Nickel(II) and copper(II) complexes have shown notable different biological activities. Nickel was long thought not to be a metal of biological importance. However, Zerner discovered that urease is a nickel enzyme [13]. Since then, other important enzymes that depend on nickel for activity have been identified. For this reason, the synthesis of complexes oriented to mimic metal sites of different types of metalloproteins constitutes an important branch in both inorganic and organic chemistry [14]. The role of copper compounds as pharmaceutical drugs in the treatment of numerous chronic diseases is well established. The macrocyclic ligands in the complexes are smaller than enzymes which allow the attack at the macromolecular region which are beyond the reach of enzymes. Due to its unique properties it is used as adjuvant in PCR diagnostics, cleaving agents and attacking agents [15, 16].

It is significant to note that pendant-arm macrocyclic nickel(II) and copper(II) complexes have been rarely used for bimetallic biosite [17, 18]. This has prompted us to

design and synthesis a series of dinuclear nickel(II) and copper(II) complexes with pendant-armed polyamine macrocycles of diethylenetriamine derivatives with N-substituted groups (at the secondary amine nitrogen atom) and 2,6-diformyl-4-methylphenol by template method. The biological significance of the synthesized pendant-armed complexes has been investigated in term of antibacterial, DNA interaction and cytotoxic activities.

2. Experimental section

2.1. Materials

2,6-Diformyl-4-methylphenol has been synthesized according to the literature method [19]. Benzoyl chloride, nitrobenzoyl chlorides, diethylenetriamine, salicylaldehyde and metal(II) perchlorate salts were commercial products (from Merck and Aldrich). Solvents were dried and purified before being used according to standard procedure. Tetra(*n*–butyl)ammonium perchlorate (TBAP) used as supporting electrolyte in the electrochemical measurements was purchased from Fluka and recrystallized from hot methanol. (***Caution***! TBAP is potentially explosive; hence care should be taken in handling the compound). Tris-HCl buffer (5mM Tris-HCl/50 mM NaCl, pH 7.2), Tris = Tris(hydroxymethyl)aminomethane, solution was prepared using deionized double distilled water. Calf thymus DNA (CT-DNA) and pBR322 DNA were purchased from Bangalore Genei (India).

2.2. Physical measurements

The elemental analysis (C, H and N) was measured with a Carlo Erba elemental analyzer Model 1106. ^{1}H NMR spectral data were collected on Varian-VNMRS-400 in $CDCl_3$ and DMSO solution with tetramethylsilane (TMS) as an internal standard at ambient temperature. IR spectra were recorded on ABB Instruments, MB-3000 spectrophotometer using KBr pellets in the range 4000–400 cm^{-1}. The mass data of ligands were obtained on a JEOL GC mate GC-MS spectrometer and the mass spectra for complexes were taken on

Q-TOF 6000 ESI mass spectrometer. Electronic spectra of complexes were recorded on Perkin Elmer Lambda-45 spectrophotometer, in the range of 200–1100 nm using 1 cm quartz micro cuvettes. X-band EPR spectra were recorded on a Varian EPR-E 112 spectrophotometer using diphenylpicrylhydrazine (DPPH) as the reference. Room temperature magnetic moments were recorded on a PAR Vibrating sample magnetometer model 155. Cyclic voltammograms were obtained on a CHI-602D electrochemical analyzer using a three-electrode cell in which a glassy carbon electrode was the working electrode, a saturated Ag/AgCl electrode was the reference electrode and platinum wire was used as the auxiliary electrode. A ferrocene/ferrocenium (1+) couple was used as an internal standard and $E_{1/2}$ of the ferrocene/ferrocenium (Fc/Fc^{+}) couple under the experimental condition was 470 mV. Tetra(*n*-butyl)ammonium perchlorate (TBAP) was used as the supporting electrolyte (0.1 M) and all complex solutions were around 10^{-3} M concentration. All electrochemical measurements were carried out in solutions purged with pure nitrogen for 30 min in advance.

2.3. Synthesis of ligands

2.3.1. 2,2'-Benzoyliminodi(ethylamine) trihydrochloride (L)

A solution of diethylenetriamine (1.08 mL, 10 mmol) in ethanol (20 mL) was added dropwise to a solution of salicylaldehyde (2.1 mL, 20 mmol) in ethanol (20 mL). The mixture was stirred for 2 h and then refluxed for 6 h. Then the reaction mixture was cooled to room temperature, and a solution of benzoyl chloride (1.16 mL, 10 mmol) in ethanol (20 mL) followed by Na_2CO_3 (1.06 g, 10 mmol) were added. The resulting solution was refluxed for 36 h, cooled to room temperature, an excess solid Na_2CO_3 was filtered off and the filtrate was concentrated. A yellowish hygroscopic product 2,2'-(benzoyliminodiethylene)bissalicylidene was obtained which was used without further purification.

Yield: 3.25 g (78%). Analytical data for $C_{25}H_{25}N_3O_3$: Selected IR (KBr) (ν/cm^{-1}): 3442 ν(OH), 1732 ν(C=O), 1631 ν(C=N). ^{1}H NMR (δ/ppm in $CDCl_3$): 2.97 (t, 8H, CH_2), 3.58

(t, 4H, CH_2), 6.86 (t, 4H, Ar-H), 7.22 (d, 4H, Ar-H), 7.30 (d, 2H, Benzylic-H), 7.44 (t, 3H, benzylic-H), 8.36 (s, 2H, CH=N), 13.46 (br s, 2H, Ar-OH).

2,2'-(benzoyliminodiethylene)bissalicylidene (3.25 g, 0.0078 mol) was suspended in 6 M HCl (50 mL). The reaction mixture was maintained under reflux for 4 h, cooled and filtered to eliminate salicylic acid. The solution was concentrated under reduced pressure up to 10 mL. The solid (L) obtained on addition of few drops of ethanol was filtered off, washed with ethanol and dried under vacuum.

L Yield: 1.36 g (55%); Colour: Pale brown; M.P: 230 °C. Analytical data for $C_{11}H_{20}Cl_3N_3O$: Calculated (%): C, 41.72; H, 6.36; N, 13.27. Found: C, 41.66; H, 6.48; N, 13.02. Selected IR (KBr) (ν/cm^{-1}): 2979 ν(NH), 1700 ν(C=O). ^{1}H NMR (δ/ppm in D_2O): 2.91 (m, 8H, CH_2), 8.40 (s, 5H, Ar-H), 10.09 (br s, NH^+). Mass EI *m/z*: 207.27 [L–3HCl].

2.3.2. 2,2'-4-Nitrobenzoyliminodi(ethylamine) trihydrochloride (L')

This compound was obtained by following the procedure similar to that for L, using 4-nitrobenzoyl chloride in place of benzoyl chloride.

2,2'-(4-nitrobenzoyliminodiethylene)bissalicylidene: Yield: 3.52 g (76%). Analytical data for $C_{25}H_{24}N_4O_5$: Selected IR (KBr) (ν/cm^{-1}): 3444 ν(OH), 1728 ν(C=O), 1632 ν(C=N), 1543, 1350 ν(NO_2). ^{1}H NMR (δ/ppm in $CDCl_3$): 3.06 (t, 4H, CH_2), 3.74 (t, 4H, CH_2), 6.85 (s, 2H, Ar-H), 6.93 (s, 2H, Ar-H), 7.20 (s, 2H, Ar-H), 7.29 (s, 2H, Ar-H), 8.21 (d, 4H, Benzylic-H), 8.29 (s, 2H, CH=N), 13.37 (br s, 1H, Ar-OH).

L' Yield: 1.45 g (52%); Colour: Brown; M.P: 220 °C. Analytical data for $C_{11}H_{19}Cl_3N_4O_3$: Calculated (%): C, 36.53; H, 63.10; N, 15.49. Found: C, 36.47; H, 36.65; N, 15.24. Selected IR (KBr) (ν/cm^{-1}): 1730 ν(C=O), 1522 ν_{asym}(NO_2), 1376 ν_{sym}(NO_2), 2900 ν(N-H stretching). ^{1}H NMR (δ/ppm in D_2O): 2.88 (m, 8H, CH_2), 8.39 (s, 4H, Ar-H), 10.02 (s, NH^+). Mass EI *m/z*: 252.27 [L'–3HCl].

2.3.3. 2,2'-3,5-Dinitrobenzoyliminodi(ethylamine) trihydrochloride (L")

This compound was obtained by following the procedure similar to that for L, using 3,5-dinitrobenzoyl chloride in place of benzoyl chloride..

2,2'-(3,5-dinitrobenzoyliminodiethylene)bissalicylidene: Yield: 3.48 g (68.8%). Analytical data for $C_{25}H_{23}N_5O_7$: 13.69. Selected IR (KBr) (ν/cm^{-1}): 3444 ν(OH), 1730 ν(C=O), 1630 ν(C=N), 1543, 1350 ν(NO_2). ^{1}H NMR (δ/ppm in $CDCl_3$): 2.83 (s, 4H, CH_2), 3.64 (s, 4H, CH_2), 6.81 (d, 4H, Ar-H), 7.25 (d, 4H, Ar-H), 8.89 (m, 3H, Benzylic-H), 8.45 (s, 2H, CH=N) 13.43 (br s, Ar-OH).

L" Yield: 1.52 g (38%); Colour: Brown; M.P: 225 °C. Analytical data for $C_{11}H_{18}Cl_3N_5O_5$: Calculated (%): C, 32.48; H, 4.46; N, 17.22. Found: C, 32.42; H, 4.58; N, 16.97. Selected IR (KBr) (ν/cm^{-1}): 2961 ν(NH), 1729 ν(C=O), 1522 ν_{asym}(NO_2), 1376 ν_{sym}(NO_2). ^{1}H NMR (δ/ppm in D_2O): 2.91 (m, 8H, CH_2), 8.41 (s, 3H, Ar-H), 10.01 (s, NH^+). Mass EI *m/z*: 297.91 [L" –3HCl].

2.4. General procedure for synthesis of pendant-armed polyamine macrocyclic dinuclear nickel(II) and copper(II) complexes

A solution of NaOH (3 mmol) in ethanol (10 mL) was added to a suspension of hydrochloride salt of the appropriate amine (**L**, **L'**, **L"**) (1 mmol) in ethanol (10 mL). The mixture was stirred at room temperature for few minutes and filtered. Then the precipitate was washed with ethanol (10 mL) and the combined filtrate was added dropwise to a solution of $M(ClO_4)_2.6H_2O$ (1.5 mmol) and 2,6-diformyl-4-methylphenol (1 mmol) in ethanol (20 mL) over a period of 30 min. The resulting solution was stirred for 4 h and refluxed for 5–7 h. The precipitate thus obtained was filtered, washed with cold ethanol, followed by diethyl ether and dried under vacuum.

2.4.1. $[Ni_2L^1](ClO_4)_2$, (1)

Yield: 0.46 g (42%); Colour: Brownish yellow. Analytical data for $[C_{40}H_{40}N_6O_4Ni_2](ClO_4)_2$ (FW = 1075.04 g/mol): Calculated (%): C, 44.69; H, 3.56; N, 10.42. Found: C, 44.70; H, 3.76; N, 10.97. Selected IR (KBr) (ν/cm^{-1}): 1645 ν(C=N), 1091 and 625 (s) ν[ClO_4^- uncoordinated]. Conductance (Λ_m/S cm^2 mol^{-1}) in DMF: 139.

2.4.2. $[Ni_2L^2](ClO_4)_2$, (2)

Yield: 0.40 g (40%); Colour: Brownish yellow. Analytical data for $[C_{40}H_{38}N_8O_8Ni_2](ClO_4)_2$ (FW = 985.05 g/mol): Calculated (%): C, 48.77; H, 4.09; N, 8.53. Found: C, 48.78; H, 4.29; N, 9.08. Selected IR (KBr) (ν/cm^{-1}): 1643 ν(C=N), 1531 $\nu_{asym}(NO_2)$, 1332 $\nu_{sym}(NO_2)$, 1092 and 624 (s) ν[ClO_4^- uncoordinated]. Conductance (Λ_m/S cm^2 mol^{-1}) in DMF: 142.

2.4.3. $[Ni_2L^3](ClO_4)_2$, (3)

Yield: 0.51 g (43%); Colour: Brownish yellow. Analytical data for $[C_{40}H_{36}N_{10}O_{12}Ni_2](ClO_4)_2$ (FW = 1165.04 g/mol): Calculated (%): C,41.23; H, 3.11; N, 12.02. Found: C, 41.24; H, 3.31; N, 12.57. Selected IR (KBr) (ν/cm^{-1}): 1647 ν(C=N), 1529 $\nu_{asym}(NO_2)$, 1340 $\nu_{sym}(NO_2)$, 1096 and 625 (s) ν[ClO_4^- uncoordinated]. Conductance (Λ_m/S cm^2 mol^{-1}) in DMF: 150.

2.4.4. $[Cu_2L^1](ClO_4)_2$, (4)

Yield: 0.52 g (50%); Colour: Green. Analytical data for $[C_{40}H_{40}N_6O_4Cu_2](ClO_4)_2$ (FW = 1021.21 g/mol): Calculated (%): C,47.04; H,3.75; N,10.97. Found: C, 47.05; H, 3.95; N, 11.52. Selected IR (KBr) (ν/cm^{-1}): 1646 ν(C=N), 1105 and 624 (s) ν[ClO_4^- uncoordinated]. Conductance (Λ_m/S cm^2 mol^{-1}) in DMF: 148. g = 2.14. μ_{eff} = 1.52 B.M.

2.4.5. $[Cu_2L^2](ClO_4)_2$, (5)

Yield: 0.56 g (60%); Colour: Green. Analytical data for $[C_{40}H_{38}N_8O_8Cu_2](ClO_4)_2$ (FW = 931.22 g/mol): Calculated (%): C, 51.59; H, 4.32; N, 9.02. Found: C, 51.60; H, 4.52; N, 9.57, selected IR (KBr) (ν/cm^{-1}): 1644 ν(C=N), 1528 $\nu_{asym}(NO_2)$, 1330 $\nu_{sym}(NO_2)$, 1103 and 625 (s) ν[ClO_4^- uncoordinated]. Conductance (Λ_m/S cm^2 mol^{-1}) in DMF: 130. g = 2.14. μ_{eff} = 1.54 B.M.

2.4.6. $[Cu_2L^3](ClO_4)_2$, (6)

Yield: 0.50 g (44%); Colour: Green. Analytical data for $[C_{40}H_{36}N_{10}O_{12}Cu_2](ClO_4)_2$ (FW= 1111.20): Calculated (%): C, 43.23; H, 3.26; N, 12.60. Found: C, 43.24; H, 3.46; N, 13.15. selected IR (KBr) (ν/cm^{-1}): 1647 ν(C=N), 1529 $\nu_{asym}(NO_2)$, 1340 $\nu_{sym}(NO_2)$, 1106 and 624 (s) ν[ClO_4^- uncoordinated]. Conductance (Λ_m/S cm^2 mol^{-1}) in DMF: 133. g = 2.15. μ_{eff} = 1.53 B.M.

2.5. *In vitro* antibacterial screening

The antibacterial activity of the pendant-armed macrocyclic nickel(II) and copper(II) complexes **1**–**6** was evaluated against one Gram –ve *Proteus vulgaris* and four Gram +ve *Enterococcus faecalis*, *Staphylococcus aureus*, *Streptococcus mutants* and *Streptococcus pneumoniae* strains by agar well diffusion method [20]. These five bacterial strains were selected on the basis of their clinical importance in causing diseases in humans. All the microbial cultures were adjusted to 0.5 McFarland standards, which is visually comparable to a microbial suspension of approximately 1.5×10^8 c.f.u./mL [21]. Five bacterial strains were pregrown in nutrient broth/Luria Bertaini broth at 37 ºC for 24 h. Nutrient/Luria Bertaini agar medium was poured into sterilized petri dishes and allowed to solidify. After solidification, 100 µL of target bacterial cell cultures were spread over the medium using a spreader and the wells were punched with 3 mm diameter gel puncher. A different concentration such as 50 µL (250 µg), 100 µL (500 µg) and 200 µL (1000 µg) of complexes was pipetted out into each

well against each test bacteria. An empty well inoculated with sterile Nutrient broth/Luria Bertaini alone served as negative controls. Inoculated plates were incubated for a day at room temperature. The experiments were performed in triplicates. The antibacterial activity of the compounds (in term of inhibition of bacterial growth) against bacterial isolates was determined from the growth in the test plates compared to the respective control plates by using the formula

$$\% I \text{ (Growth inhibition)} = 100(C\text{-}T)/C$$

Where C is the diameter of bacterial growth in control plate and T is the diameter of bacterial growth in test plate.

2.6. DNA Interaction experiments

2.6.1. Electronic absorption titration

The binding analysis of complexes **2**, **3**, **5** and **6** with CT-DNA was performed at room temperature. The absorption titration experiments of complexes with CT-DNA was characterized by measuring their effects on the UV-Vis spectroscopy. The complexes were dissolved in a mixed solvent of Tris-HCl/NaCl buffer (pH 7.2) containing 5% DMF (solution was prepared using doubly distilled water). A solution of CT-DNA in the buffer gave a ratio of UV-Vis absorbance at 260 and 280 nm (A_{260}/A_{280}) of ca 1.8 indicating that the CT-DNA was sufficiently free of protein [22]. Electronic absorption titrations were performed with a fixed concentration of metal complexes (100 µM) while gradually increasing the nucleotide concentration from 0 to 40 µM. Due correction was made for the absorbance of DNA itself. Absorbance values were recorded after each successive addition of DNA solution and equilibration (ca.10 min). The absorbance band of complexes that get shifted significantly due to the addition of CT-DNA was chosen to monitor as an indication of the binding between them. From the obtained data, the intrinsic binding constant K_b of the metal complexes with CT-DNA was determined using the equation [23],

$$[DNA]/(\varepsilon_a - \varepsilon_f) = [DNA]/(\varepsilon_b - \varepsilon_f) + 1/K_b(\varepsilon_b - \varepsilon_f)$$

Where, [DNA] is the concentration of CT-DNA in base pairs, ε_a is the extinction coefficient of complex at a given DNA concentration, ε_f is the extinction coefficient of complex in free solution and ε_b is the extinction coefficient of complex when fully bound to DNA. A plot of $[DNA]/(\varepsilon_b - \varepsilon_f)$ *versus* [DNA] gave a slope and an intercept equal to $1/(\varepsilon_a - \varepsilon_f)$ and $1/K_b(\varepsilon_b - \varepsilon_f)$, respectively. The intrinsic binding constant K_b is the ratio of the slope to the intercept.

2.6.2. Fluorescence quenching studies

The binding constant of complexes can also be determined by fluorescence quenching experiments using a reference ethidium bromide (EB) bound to CT DNA solution of 5% DMF in Tris–HCl/NaCl buffer (pH 7.2). The changes in fluorescence intensities at 605 nm (545 nm excitation) of EB bound to DNA were measured with different complex concentrations. EB was non emissive in Tris–HCl/NaCl buffer (pH 7.2) due to fluorescence quenching of the free EB by the solvent molecules. In the presence of DNA, EB showed enhanced emission intensity due to its intercalative binding to DNA. A competitive binding of the metal complexes to CT DNA resulted in the displacement of the bound EB, thereby decreasing its emission intensity. Stern-Volmer quenching constant [24] was calculated using the equation $I_o/I = 1 + K_{sv}[Q]$ where, I_o is the emission intensity of EB-DNA in the absence of complex, I is the emission intensity of EB-DNA in the presence of complex, [Q] is the concentration (10 μM) of quencher. K_{sv} is a linear Stern-Volmer constant given by the ratio of slope to intercept in the plot of I_0/I *versus* Q.

2.6.3. Electrochemical titration

Electrochemical properties of complexes with CT-DNA were studied by cyclic voltammetry in Tris-HCl/NaCl buffer solution (pH = 7.2) using tetra(*n*-butyl)ammonium perchlorate (TBAP) as supporting electrolyte. The concentration of complexes can be taken

as 100 µM and 200 µM for DNA. Solutions were deoxygenated by purging with N_2 gas for 10 min prior to measurements.

2.6.4. DNA Cleavage analysis

DNA cleavage was monitored by agarose gel electrophoresis using the reaction mixture containing 1 µg of supercoiled DNA pBR322, 250 µg of the pendant-armed macrocyclic complexes **1**–**6**, 2 µL of 1% DMSO (Reactive oxygen species (ROS) scavenger) and 5 µL of hydrogen peroxide (40 mmol, oxidizing agent). After incubation at 37 ºC for 2 h, 2 µL of loading buffer (0.25% bromophenol blue, 0.25% xylene cyanol, 30% glycerol in H_2O) was added to each tube . The agarose gel (1 %) containing 1 µg of ethidium bromide (EB) was prepared and the electrophoresis of the DNA cleavage products was performed on it. The gel was run at 60 V for 2 h in *Tris*-borate EDTA (TBE) buffer (89 mM Tris-borate, pH 8.3, 1 mmol EDTA) and the bands were identified by placing the stained gel under an illuminated UV lamp. After electrophoresis, the proportion of both the cleaved and uncleaved DNA in each fraction was quantitatively estimated on the basis of the band intensities using gel documentation system (BIO RAD). The intensity of each band relative to that of the plasmid supercoiled form was multiplied by 1.43 to take account of the reduced affinity for ethidium bromide [25].

2.7. Cell Proliferation assay

2.7.1. Cell lines and cell culture

Human liver adenocarcinoma (HepG2) cell line was obtained from National Centre for Cell Science (NCCS), Pune, India. Cells were cultured in Dulbecco's modified eagle medium (DMEM) (St. Louis, Mo, USA) supplemented with 10% (V/V) fetal bovine serum (FBS) , penicillin 100 µg/mL, streptomycin 20 µg/mL, Kanamycin acid sulphate 20 µg/mL and 7.5% sodium bicarbonate solution. The cells were maintained as monolayers in 25 cm^2

plastic tissue culture flask at 37 ºC in a humidified atmosphere containing 5% CO_2 in air. Exponentially growing cells were used in all the experiments.

2.7.2. Cell viability assay

The cell viability of complexes **2**, **5** and **6** was assessed by MTT (3-(4,5-dimethylthiazol-2-yl)-2,5-diphenyltetrazolium bromide) assay as described by Mosmann [26] . In order to detect the cytotoxicity, the HepG2 cells were grown in DMEM medium containing 10% FBS. For screening experiments, the cells (5×10^3 cells/well) were plated in 96-well plates with the medium containing 10% FBS and incubated for 24 h under 5% CO_2, 95% O_2 at 37 ºC. Later, the medium was replaced with DMEM containing 1% FBS and complexes **2**, **5** and **6** (10, 8 and 2 µg/mL, respectively) dissolved in DMSO were added to the cells incubated at 37 ºC in 5% CO_2. The test samples were kept in triplicate. Controls were maintained under similar conditions without the influence of compounds under study. After 24 and 48 h, MTT stock solution (5 mg/mL) in phosphate buffer saline (PBS) was added to each culture well, equal to one tenth of the original culture volume and the plates were wrapped with aluminium foil and incubated at 37 ºC for 4 h. At the end of the incubation period, the medium was removed and the purple formazan product was dissolved by adding of 100 µL of DMSO to each well and the absorbance was measured at 570 nm using a multiplate reader. The % of cell viability was evaluated using the following equation:

$$\% \text{ Cell viability} = [A_{570}\,(\text{sample})/A_{570}\,(\text{control})] \times 100$$

Where A_{570} (sample) refers to the reading from the wells treated with complexes and A_{570} (control) refers to that from the wells treated with medium containing 10% FBS. From this plot, the IC_{50} values was calculated.

2.7.3. Apoptosis studies

Apoptosis studies were performed with a staining method utilizing propidium iodide (PI). HepG2 cells plated at a density of 5×10^4 cells/well into a six well chamber plate. At

>90% confluence, the cells were treated with complexes **2**, **5** and **6** at IC_{50} dose for 24 h. The cells were washed with PBS fixed methanol and acetic acid (3:1, v/v) for 30 min and stained with 50 µg/mL propidium iodide for 20 min. Nuclear morphology of apoptotic cells with condensed/fragmented nuclei was examined under a fluorescent microscope and at least 1×10^3 cells were counted to assess apoptotic cell death.

2.7.4. Alkaline single-cell gel electrophoresis (Comet assay)

A comet assay was performed to determine the degree of oxidative DNA damage induced by complexes. Adenocarcinoma cells were exposed to complexes **2**, **5** and **6** for 24 h and washed with phosphate buffer saline (PBS). The cells suspension was mixed with 75 µL of 0.5% low melting agarose (LMA) at 39 ºC and spread on a fully frosted microscopic slide pre-coated with 200 µL of 1% LMA and then immersed in lytic solution (2.5 M NaCl, 10 mM Na-EDTA, 10 mM Tris–base and 0.1% Trion X-100, 10% DMSO; the last two compounds were added fresh, pH 10) for 1 h at 4 ºC. The slides were then placed in a gel electrophoresis apparatus (containing 300 mM NaOH and 10 mM Na-EDTA, pH 13) for 40 min to allow unwinding of DNA and the alkali labile damage. Next, an electrical field (3000 mA, 25 V) was applied for 20 min at 4 ºC to draw the negatively charged DNA towards an anode. After electrophoresis, slides were washed thrice for 5 min at 4 ºC in a neutralizing buffer (0.4 M Tris, pH 7.5), followed by staining with 75 µL of propidium iodide (40 µg/mL) and then the slides were examined using fluorescence microscope at 20X magnification. The DNA contents in the head and tail were quantified by using CASP software.

3. Results and Discussion

For synthesis of ligands (L, L' and L"), salicylaldehyde was utilized to protect the two primary amino groups of diethylenetriamine from nucleophilic additions so that the benzoylation reaction can take place only at the secondary amine and the resulting ligands was isolated as its hydrochloride salt (**Scheme 1**). The Schiff base condensation of ligands and 2,6-diformyl-4-methylphenol with appropriate hydrated metal(II) perchlorate salt (1:1:1.5 mole ratio) in ethanol gave good yields of analytically pure dinuclear pendant-armed macrocyclic nickel(II) and copper(II) complexes (**Scheme 2**). All the complexes were characterized by elemental analyses consistent with the formulations given in experimental section. All the complexes are air stable solids, soluble in CH_3CN, DMF and DMSO. Our attempt to synthesize macrocyclic ligands in the absence of metal ions was unsuccessful and cyclocondensation reactions did not occur, therefore we tried different metal ions in order to examine the effect of the template reaction on the occurrence of ring closure. Our results clearly demonstrate that the nature of the metal template determines the outcome of the Schiff-base condensation between 2,6-diformyl-4-methylphenol and a difunctional amine component.

3.1. Spectral and magnetic studies

The IR spectra provide valuable information regarding the coordination behavior of the ligand to the metal ion. All the ligands show a sharp band in the region 1597 cm^{-1} due to NH_3^+ group of the salt of a primary amine [27]. The IR spectra of ligands show a band in the region of 1700–1730 cm^{-1} due to the ν(C=O) vibration. The spectra of complexes revealed significant differences from those of free ligands as described below. The formation of complexes of macrocyclic framework is confirmed by the absence of bands characteristic of starting materials: the band due to NH_3^+ group in the region 1597 cm^{-1} and the aldehydic -C=O band at 1680 cm^{-1} disappeared and band for imine stretching appear as sharp

band in the region 1643–1647 cm^{-1}. The band due to benzoylic ν(C=O) stretching vibrations are absent in the IR spectra of all complexes suggesting the involvement of this group in coordination to the metal. A strong absorption in the region of 1528–1531 and 1330–1340 cm^{-1} corresponds to NO_2 stretching vibrations. The bands at 1440–1485 cm^{-1} were assigned to aromatic ring vibrations and appeared in the same position on complexation with respect to free ligands. The presence of uncoordinated perchlorate anions in all the binuclear complexes are inferred from single broad band around 1100 cm^{-1} (ν_3-antisymmetric stretching) which are not split and a band around 625 cm^{-1} (ν_4-antisymmetric bending). The band around 930 cm^{-1} (ν_2-symmetric stretching) due to coordinated perchlorate is not observed and this clearly indicates that no perchlorate ions are coordinated in the complexes [28].

The ^{1}H NMR spectra of ligands recorded in DMSO-D_6 show well resolved signals as expected (**Fig. 1)**. The aromatic region shows a sharp singlet at δ 8.3 ppm assigned to the aromatic protons, and a multiplet at δ 3.3 ppm due to methylene protons. The NH^{3+} and NH^{+} proton of the ammonium group shows a broad singlet at δ 10.0 ppm. In the mass spectra, the calculated and observed isotropic patterns are in good agreement. The high resolution mass spectral data of all the ligands confirm the proposed formulae. The different fragments of the ligand gave peaks with various intensities at different *m/z* values. **Fig. 2** depicts the mass spectrum of L", and its fragmentation pattern is depicted in **Fig. S1**. The ESI mass spectral data of all complexes were studied in positive mode in CH_3CN solution and provided strong evidence for the formation of the macrocyclic dinuclear complexes. **Fig. 3** depicts the mass spectrum of complex **3** and its fragmentation pattern is depicted in **Fig. S2**. The *m/z* peak at 967 corresponds to molecular weight of complex **3**. The intensities of peaks are in accordance with the abundance of the ions. The observed molecular ion corresponds to the mass of entire complex excluding two counter ions, perchlorate.

The electronic spectra of all the binuclear complexes (**1**–**6)** were recorded in DMF medium and the spectral data are given in **Table S1.** The absorption spectra of complexes exhibit an intense peak in the range of 232–275 nm assigned to the intra ligand charge transfer transition ($\pi - \pi^*$). A medium intensity broad band in the range of 376–409 nm is due to ligand to metal charge transfer transition. Complexes **1-3** show three d-d transition bands centered at 643–657, 759–771 and 922–935 nm, which are characteristic of Ni^{2+} in the six coordination environment of the binuclear complexes whereas complexes **4**–**6** exhibit one d-d transition band between 553–587 nm. The electronic spectral features strongly suggest that the six coordination geometry around the metal ion in the binuclear complexes might be distorted octahedral [29].

The EPR spectra of dinuclear copper(II) complexes **4**–**6** were recorded on X-band frequency 9.4 GH_Z under magnetic field strength 3200 G at room temperature (**Fig.S3** & **S4**). The g values were evaluated using the relationship $h\nu = g\beta H$. A broad band centered at g = 2.14–2.15 attributed to the antiferromagnetic interaction between two copper nuclei arises from the spin-spin coupling of the electrons of both the copper ions [30]. The observed room temperature magnetic moment values for complexes **4**–**6** range between 1.52–1.54 BM, lower than the spin only value. This clearly indicates the occurrence of an antiferromagnetic exchange interaction between the two copper(II) ions. Magneto structural correlation in phenoxo-bridged dicopper(II) complexes reveal that the dominant pathway for superexchange interaction through the oxygen atom involves interaction of the two copper $d_{x^2-y^2}$ orbitals and the *p* orbitals on the oxygen [31].

3.2. Electrochemical studies

The molar conductance values for complexes **1**–**6** in DMF are in the range 130–170 Λ_m/S cm^2 mol^{-1} indicative of 1:2 electrolyte type [32]. The electrochemical properties of complexes were studied by cyclic voltammetry in DMF containing 10^{-3} M

tetra(*n*-butyl)ammonium perchlorate as supporting electrolyte. This technique is based on varying an applied potential at a working electrode in both forward and reverse directions (at some scan rates) while monitoring the current. The electrochemical properties of the complexes depend on number of factors such as chelate ring/size, axial ligation, degree and distribution of unsaturation and substitution pattern in the chelate ring [33].

3.2.1. Reduction process at cathodic potential

The cyclic voltammograms of complexes **1-6** at cathodic potential was recorded in the potential range from 0 to –2.0 V (**Fig S5)**. The electrochemical data are summarized in **Table S2**. The first reduction potential (E^1_{pc}) ranges from −0.62 to −0.76 V and the second reduction potential (E^2_{pc}) lies in the range of –1.21 to –1.31 V. These two reduction waves correspond to stepwise one-electron reductions through a $M^{II}M^{I}$ intermediate to give binuclear $M^{I}M^{I}$ species. The reason for the observed two reduction waves may be due to electronic exchange between the metal ions; after the first one-electron reduction, some of the electron density is transferred from the reduced metal ion to the other metal ion, and hence the second reduction appears at a high negative potential. The two reduction processes are assigned as follows:

$$M^{II}M^{II} \rightarrow M^{II}M^{I} \rightarrow M^{I}M^{I}$$

3.2.2. Oxidation process at anodic potential

All the nickel(II) complexes **1**–**3** show two oxidation processes in the range of 1.08 to 1.74 V. The cyclic voltammogram of the dinuclear nickel(II) complexes is shown in **Fig. S6** and the data are summarized in **Table S2**. The first oxidation potential (E^1_{pa}) ranges from 1.08 to 1.14 V while the second oxidation potential (E^2_{pa}) lies in range of 1.71 to 1.74 V. The two irreversible oxidation waves correspond to each one-electron transfer process for complexes. Controlled potential electrolysis experiment indicates that the two oxidation peaks are associated with stepwise oxidation process at nickel(II) center.

$$Ni^{II}Ni^{II} \rightarrow Ni^{III}Ni^{II} \rightarrow Ni^{III}Ni^{III}$$

3.3. Biological studies

3.3.1. *In vitro* antibacterial screening

The *in vitro* antibacterial screening of complexes **1**–**6** were performed at fixed concentration of 150 µg/mL and the results obtained were compared with standard antibiotic, ciprofloxacin. The mean zone of inhibition values of the investigated complexes are shown in **Fig. S7** & **S8** and the data are summarized in **Table 1.** The antibacterial activities of complexes follow the order **6** > **5** > **4** and **3** > **2** > **1** for copper (II) and nickel(II) complexes, respectively. Among these, complex **6** shows good antibacterial activity and **1** shows lowest activity against tested microorganisms, when compared with the standard drug. Complexes containing dinitro substituents (**3** & **6**) in the pendant-arm show maximum antibacterial effect while minimum activity was exhibited by the complexes without substituents (**1** & **4**) in the pendant-arm. The reason for high antibacterial activity of copper(II) complexes can be explained in terms of the effect of copper(II) metal ion on the normal cell process. The complexation reaction reduces the polarity of the metal ion by partial sharing of metal ion positive charge with donor atoms present in the pendant-armed macrocycles and there may be π −electron delocalization over the whole chelate ring. This increases the lipophilic character of the metal chelate and favours its permeation through the lipid layer of the bacterial cell membranes. These complexes also disturb the respiration process of the cell and thus block the synthesis of proteins that restricts further growth of the organism and as a result microorganisms die [34].

It is also assumed that the increase in antibacterial activity is due to the factors such as dipole moment, conductivity, solubility and cell permeability mechanism influenced by the presence of metal ion [35]. The antibacterial activity of complexes **1-6** are comparable to series of N-benzoylated tetraaza macrocyclic complexes reported in the literature [18].

3.3.2. DNA binding studies

3.3.2.1. Absorption spectroscopic studies

DNA being one of the most important targets of many anticancer agents, designing and developing metal complexes that avidly bind to DNA are of paramount importance [36]. Electronic absorption spectroscopy is an effective method to examine the binding mode and strength of metal complexes with DNA. In general, hypochromism and/or bathochromism or hypsochromism are associated with the binding of metal complexes to the DNA helix, due to the intercalative mode involving a strong stacking interaction between the aromatic chromophore of complexes and the base pairs of DNA. The extent of hypochromism is generally consistent with the strength of the intercalative interaction [37]. In the present investigation, the interaction of the pendant-armed binuclear nickel(II) (**2** & **3**) and copper(II) (**5** & **6**) complexes with CT-DNA in Tris-HCl/NaCl buffer was performed by monitoring the fixed complex concentration (10 μM, in 5% DMF) to which increments of DNA stock solutions (from 0 to 100 μM) was added. The absorption spectra of complexes in the absence and presence of CT-DNA at different concentrations are given in **Fig. 4** & **5.** With increasing concentration of duplex DNA to complexes, the absorption gradually decreased along with a small amount of red-shift, indicating the interaction of aromatic N-containing pendant macrocycles with CT-DNA. The intrinsic binding constant K_b for each complex has been obtained from the plot of [DNA]/($\varepsilon_a - \varepsilon_f$) *versus* [DNA] (**Table 2)**. The binding constants follow the order **6** > **5** > **3** > **2** and indicate intercalation between complexes and CT-DNA. The high binding nature of the metal complexes may be due to the additional π–π* interaction through the aromatic phenyl rings. Upon intercalation, the π* orbital of the intercalated ligand may couple with the π orbital of the base pairs of DNA, thus decreasing the π–π* transition energy leading to bathochromism. On the other hand, the coupling π orbital is partially filled by electrons, which decrease the transition probabilities and concomitantly leads to

hypochromism. The complex **6** interacts with DNA to the greatest degree, with binding constant K_b of 8.5×10^2 M^{-1}. The higher DNA binding ability of copper complexes, in particular, can be assigned to its biocompatibility, high nucleobase affinity, and capacity to possess biologically accessible redox potentials. It can recognize nucleic acids, in a sequence-specific fashion and bind to them in such a way that their functioning will be altered [38]. These values are very distinctive of metal-based compounds that bind to DNA *via* intercalation. The DNA-binding constant of the title complexes are comparable to those of reported pendant-armed macrocyclic binuclear metal(II) complexes [39, 40].

3.3.2.2. Ethidium bromide quenching assay

Fluorescence quenching is a useful method to monitor the molecular interactions of chemical and biological systems because of its high sensitivity. In the present study, we have investigated the competitive binding of ethidium bromide *versus* the synthesized pendant-armed complexes (**2**, **3**, **5** & **6**) with calf thymus DNA using fluorescence spectroscopy to get better insight of DNA binding events. Ethidium bromide (EB) is one of the most sensitive fluorescence probes that can bind with DNA. The fluorescence of EB increases in the presence of DNA due to its strong intercalation between the DNA base pairs. If the complex displaces EB from the DNA-bound EB, the fluorescence intensity decreases due to the fact that the free EB molecules are much less fluorescent than the DNA bound EB molecules because the surrounding water molecules quench the fluorescence of free EB [41, 42]. The emission spectra of EB bound to CT-DNA in the absence and presence of each complex have been recorded for [EB] = 10 μM, [complex] = 0–100 μM and the DNA concentration of 10 μM. The representative emission spectra of complexes **2**, **3**, **5** & **6** upon excitation at different wavelength are given in **Fig. 6** & **7**. In the present work, the fluorescence intensity of the DNA-bound EB decreases slowly on increasing the concentration of the pendant-armed nickel(II) and copper(II) complexes. This may be due to

the displacement of the EB molecule from the intercalating site by the pendant-armed complexes. The results reveal that all complexes bind with DNA by intercalation mode.

The quenching of EB bound to DNA by the pendant-armed complexes is in good agreement with the linear Stern-Volmer equation which confirms that complexes are bound to DNA. The ratio of the slope to the intercept obtained by plotting I_o/I *versus* [Complex] yielded the value of K_{sv} (**Table 2**). The fluorescence quenching efficiency follows the order **6 > 5 > 3 > 2** indicating a higher quenching by copper(II) complexes as compared to nickel(II) complexes. These values suggest that complex **6** showed higher quenching efficiency than the other complexes **2, 3** and **5**. The ratio of quenching of the intensities in all four complexes is different, reflecting more binding of complex **6** with CT-DNA to leach out more number of EB molecules originally bound to DNA than that of complexes **2, 3** and **5**. The high K_{sv} values of complexes reveal the intercalative binding of complexes with CT-DNA. The hydrophobic property of these complexes containing 4-methylphenol group facilitates the DNA binding. The enhancement of emission intensity is indicative of binding of these complexes to the hydrophobic pocket of DNA, since the hydrophobic environment inside the DNA helix reduces the accessibility of water molecules to complex and the mobility of complexes is restricted at the binding site, leading to decrease of vibrational modes of relaxation. These results are in agreement with the results obtained from UV-Vis spectra.

3.3.2.3. Electrochemical titration

The application of cyclic voltammetry provides useful compliment to the previously utilized methods of investigation such as UV-Vis and fluorescence quenching experiments to study interaction between complexes and DNA. It is a very sensitive analytical technique to determine changes in redox behavior of metallic species in the presence of biologically important molecules and thus the nature and mode of DNA binding of metal complexes. In

general, when the metal complex binds to DNA *via* intercalation, the potential presents a positive shift, while in the case of electrostatic interaction, the potential will shift to a negative direction. If more than one potential exist simultaneously, a positive and negative shift of E_p^1 and E_p^2, respectively, the molecule can bind to DNA by both intercalation and electrostatic interaction [43].

The typical cyclic voltammograms of complexes **2**, **3**, **5** and **6** in the absence and presence of CT-DNA are shown in **Fig. 8** and the data are summarized in **Table 3**. No new reduction waves appeared on the incremental addition of CT-DNA to complex, but the cathodic peak current of complexes decreases, suggesting that CT-DNA moiety is bound strongly to complex. The observed decrease in current intensity is attributed to the diffusion of an equilibrium mixture of free and DNA-bound complex to the electrode surface and suggests the existence of the same electrochemical behaviour upon addition of CT-DNA. The slower mass transfer of complex bound to DNA fragments leads to a decrease in concentration of the unbound redox active species in solution. The considerable decrease in voltammetric current (i_{pc}^1 = 0.70 to 1.50 µA; i_{pc}^2 = 0.80 to 1.45 µA) and positive shift (E_{pc}^1 = –0.69 to –0.75 V; E_{pc}^2 = –1.20 to –1.26 V) suggests the existence of intercalation mode of binding between complex and nitrogenous bases of DNA. However, according to Kelly and coworkers [44], the drop of peak currents is due to the reason that the complex bound to DNA and the product was nonelectroactive, decreasing the concentration of electroactive species in solution and resulting in the drop of the peak currents. These positive shifts are considered to be evidenced for intercalation of complexes with DNA due to hydrophobic interactions.

3.3.3. DNA cleavage studies

. There are number of agents which exert their effect by inhibiting enzymes that act upon DNA. These inhibitions result from the binding of such agents to the enzyme site of

interaction on the DNA rather than to direct enzyme inactivation. Transition metals have been reported to inhibit DNA repair enzymes. The DNA cleavage efficiency of complex is attributed to the different binding affinity of complex to DNA. There has been considerable interest in DNA cleavage reactions activated by transition metal complexes. The delivery of metal ion to the helix, in locally generating oxygen or hydroxide radicals, yields an efficient cleavage reaction [45]. Gel electrophoresis is a technique based on the migration of DNA under the influence of an electric potential. When the original supercoiled form (Form I) of plasmid DNA is nicked, an open circular relaxed form (Form II) will exist in the system and the linear form (Form III) can be found upon further cleavage. When circular plasmid DNA is run on horizontal gel by electrophoresis, the compact Form I migrates relatively faster while the nicked Form II migrates slowly, and the linearised Form III migrates between Forms I and II.

The DNA cleavage ability of complexes **1**–**6** was monitored by agarose gel electrophoresis on plasmid pBR322 DNA as a substrate in a medium of 5 mM Tris-HCl/50 mM NaCl buffer (pH 7.2) under aerobic conditions with H_2O_2 as an oxidant. Incubation of pBR322 DNA with complexes for 2 h at 37 ºC results in extensive cleavage of DNA, the supercoiled Form I is first degraded to Form II (relaxed circular) and then to Form III (linear) in the presence of 100 µM of complex. The loaded pendant-armed complexes damage DNA more efficiently in the presence of an oxidant and form DNA adducts that migrate at different rates (**Fig. 9** & **S9**). This may be attributed to the formation of hydroxyl free radicals which participate in the oxidation of the deoxyribose moiety, followed by hydrolytic cleavage of a sugar phosphate back bone. All complexes showed pronounced cleavage activity in the presence of H_2O_2 which may be due to the increased production of hydroxyl radicals. At the same time, the cleavage was diminished significantly in the presence of free-radical scavenger (DMSO), implying that hydroxyl radicals mediate

the cleavage. This provides clear evidence for the involvement of hydroxyl radicals in the DNA strand scission performed by M(II) complexes. These results indicate that the metal ions play an important role in the cleavage of isolated DNA. As the compounds were observed to cleave DNA, it can be concluded that these compounds inhibit the growth of pathogenic organism by cleaving the genome.

3.3.4. Cytotoxicity evaluation

3.3.4.1. MTT assay

The cytotoxicity of complexes **2, 5** and **6** against human liver adenocarcinoma (HepG2) cell line has been investigated by using MTT reduction assay. The assay was based on the mitochondrial reduction of the tetrazolium salt by actively growing cells to produce blue water insoluble formazan crystals, i.e., only live cells reduce yellow MTT to blue formazan products but not dead cells. The observed IC_{50} values (**Table 2**) of the complexes **2**, **5** and **6** at 24 h are lower than those at 48 h indicating that they are dose and time dependent (**Fig. 10)**. Further, as revealed by the observed IC_{50} values, the potency of the complexes to kill the cancer cells follows the order **6 > 5 > 2**, revealing that it varies with the mode and extent of interaction of the complexes with DNA. Interestingly, the complex **6** is more potent than the complexes **2** and **5**. The complexes producing a higher mortality with lower concentration at short duration of time compared to others with higher concentration and longer time duration. It is commonly believed that the biological activities of anticancer metal complexes are dependent on their ability to bind DNA and damage its structure resulting in the impairment of its function, [46] which is followed by inhibition of replication and transcription processes, and eventually cell death, if the DNA lesion are not properly repaired.

3.3.4.2. Cytomorphology observation

Microscopic observations were monitored using Nikon light inverted microscope wherein treated cells showed distinct cellular morphological changes indicating unhealthy cells, whereas the control appeared normal (**Fig. 11**). Control cells were irregular confluent aggregates with rounded and polygonal cells. Synthesized pendant-armed treated cells appeared to shrink, became spherical in shape and cell spreading patterns were restricted when compared to control.

3.3.4.3. Apoptotic activity

Apoptosis (programmed cell death) and necrosis (accidental cell death) are two types of cell death. Necrotic cells undergo cell lysis and lose their membrane integrity and induce severe inflammation. Apoptosis plays a major role during the development and homeostasis. Apoptosis is a process of gene-mediated programmed cell death essential for the elimination of unwanted cells in various biological systems and no inflammatory response is found. Harmless removal of cells (says, cancer cells) is one consideration in chemotherapy. Therefore, apoptosis is one of the considerations in the development of anticancer drugs. The sequence of changes in cellular morphology of apoptosis includes oligo-nucleosomal DNA fragmentation, nucleus condensation, DNA leddering and PARP-1 cleavage [47–49]. Apoptosis studies of complexes **2, 5** and **6** at IC_{50} concentration was performed with a staining method utilizing propidium iodide (PI) which helps to detect difference in membrane integrity between necrotic and apoptotic cells (**Fig. 12**). With the difference in concentration gradient of complexes, the increase in the apoptotic nuclear morphology such as extensive chromatin aggregation or nuclear condensation was observed in the treated cells, and even nuclear fragmentation was found, indicating that the HepG2 cell died through an apoptosis process. The cytological changes observed are classified into four types according to the fluorescence emission and morphological features of chromatin condensation in the PI

stained nuclei: (i) viable cells have uniformly green fluorescing nuclei with highly organized structure; (ii) early apoptotic cells (which still have intact membranes but have started undergoing DNA fragmentation) have green fluorescing nuclei; but peri-nuclear chromatin condensation is visible as bright green patches or fragments; (iii) late apoptotic cells have orange red fluorescing nuclei with condensed or fragmented chromatin; and (iv) necrotic cells, swollen to large sizes, have uniformly orange to red fluorescing nuclei with no indication of chromatin fragmentation [50]. The morphological changes observed for **6** suggest that the cells are committed to apoptotic cell death more efficiently compared to complexes **2** and **5**.

The mechanism of cell death in the HepG2 liver cancer cell line appears to be apoptosis, as evidenced by PI staining, which identifies early and late apoptotic changes in cells.

3.3.4.4. Comet assay

The single-cell gel electrophoresis (comet assay) allows detection of DNA fragmentation in single cells, and was initially used for DNA damage estimation [51]. **Fig. 13** showed the effect of pendant-armed complexes **2**, **5** and **6** on HepG2 cells on DNA damage and tail length. The comet tail length was analyzed by CASP software (**Fig. S10**). As can be seen in the representative photos from fluorescence microscopy, the nucleoids of control cells were uniformly spherical in shape, reflecting the absence of any DNA damage. However, upon complete scoring of the nucleoids in experiments, reflecting a baseline level of DNA single-strand breaks. Hence, the average comet score of tail DNA for control HepG2 cells was 0.10%. In contrast, other representative photos (**Fig. 13 b**, **c** & **d)** for 24 h at IC_{50} values show significant numbers of nucleoids with larger comet tails, indicative of higher levels of DNA single-strand breaks. The comet assay scores of tail DNA were 65.14%, 75.56% and 88.48% for complexes **2**, **5** and **6**, respectively. Therefore, Pendant-armed complexes

significantly increased number of tail DNA, tail length, tail moment and olive tail moment in HepG2 liver adenocarcinoma cell line when compared to untreated cells. The results showed that percentage (**Table 2**) of cells with tail DNA increased significantly after the cells were treated with complexes **2**, **5** and **6**. The high level of DNA damage induced by complex **6** reinforces the results obtained using MTT assay and PI staining assay.

Conclusion

A series of pendant-armed polyamine macrocyclic dinuclear nickel(II) and copper(II) complexes **1**–**6** have been synthesized by template cyclocondensation of 2,6-diformyl-4-methylphenol with three different benzoyl pendant-arms, 2,2'-benzoyliminodi(ethylamine) trihydrochloride (L), 2,2'-4-nitrobenzoyliminodi(ethylamine) trihydrochloride (L') and 2,2'-3,5-dinitrobenzoyliminodi(ethylamine) trihydrochloride (L"). The *in vitro* antibacterial tests revealed that all complexes possess potent antibacterial activities toward Gram-positive and Gram-negative bacteria. The order of increasing antibacterial activities was **6 > 5 > 4 > 3 > 2 > 1**. The results of DNA binding studies suggest that the complexes bound with CT-DNA through intercalation mode. The binding constants K_b and K_{sv} follows the same order of binding affinity towards CT-DNA as **6 > 5 > 3 > 2.** The agarose gel electrophoresis studies show that complexes can promote the oxidative cleavage of plasmid DNA at physiological pH and temperature in the presence of H_2O_2. The higher DNA cleavage efficiency of the copper(II) complexes may be considered due to the increased binding ability of complexes to DNA. In cytotoxicity research, complexes **2**, **5** and **6** showed high *in vitro* cytotoxic properties against human liver adenocarcinoma cell (HepG2). From the observed IC_{50} values, the potency of complexes to kill the cancer cells follows the order **6 > 5 > 2**. These complexes bring about apoptosis of the cancerous cell line in a dose and time dependent manner. Alkaline single-cell electrophoresis (comet assay) shows that these pendant-armed complexes indeed induce DNA fragmentation, which is a further evidence of apoptosis. The

results obtained from the present work would be helpful to design and develop new pendant-armed macrocycles as potent therapeutic and antitumor agents for some major diseases.

Acknowledgements

The authors gratefully acknowledge Dr. N. Sengottuvelan, Department of Chemistry, Alagappa University, Karaikudi–630 004, India for his fruitful discussions on DNA interaction studies.

References

[1] L. Botana, R. Bastida, A. Macias, L. Valencia, Inorg. Chim. Acta 362 (2009) 3351–3356.

[2] E.C. Constable, Coordination Chemistry of Macrocyclic Compounds,E.C. Constable, Ed., Oxford University Press Inc., New York, 1999.

[3] D.K. Cabbiness, D.W. Margerum, J. Am. Chem. Soc. 91 (1969) 6540–6541.

[4] E. Kimura, Y. Kotake, M. Shionoya, Inorg. Chem. 29 (1990) 4991–4996.

[5] Z. Wei, Y. Peng, D.L. Hughes, J. Zhao, L. Huang, X. Liu, Polyhedron 69 (2014) 181-187.

[6] M.C. Fernandez-Fernandez, R. Bastida, A. Macias, J. Organomet. Chem. 694 (2009) 3608–3613.

[7] S. Gou, M. Qian, Q. Zeng, Inorg. Chim. Acta 305 (2000) 83–90.

[8] M.C. Fernandez-Fernandez. R. Bastida, A. Macias, L. Valencia, P.P. Lourido, Polyhedron 25 (2006) 783–792.

[9] S. Thyagarajan, N.N. Murthy, A.A.N. Sarjeant, K.D. Karlin, S.E. Rokita, J. Am. Chem. Soc. 128 (2006) 7003–7008.

[10] A. Arbuse, M. Font, M.A. Martinez Xavier Fontrodona, M.J. Prieto, V. Moreno, X. Sala, Inorg. Chem. 48 (2009) 11098–11107.

[11] Y. F. Chen, M. Liu, J.W. Mao, H.T. Song, H. Zhou, Z.Q. Pan, J. Coord. Chem. 65 (2012) 3413–3423.

[12] Y. Inowye, T. Kanamori, T. Yoshida, M. Shionoya, T. Koike, E. Kimura, Biol. Pharm. Bull. 17 (1994) 243–250.

[13] B. Zerner, Bioorg. Chem. 19 (1991) 116–131.

[14] C. Nunez, R. Bastida, A. Macias, L. Valencia, J. Ribas, J. L. Capelo, C. Loderio, J. Chem. Soc., Dalton Trans. 39 (2010) 7673–7683.

[15] M. Wu, D. Stoermer, T.D. Tullius, C.A. Townsend, J. Am. Chem Soc. 122 (2000) 12884–12885.

[16] M.C.B. Oliveria, M.S.R. Couto, P.C. Severino, T. Foppa, G.T.S. Martins, B. Szpoganicz, R.A. Peralta, A. Neves, H. Terenzi, Polyhedron 24 (2005) 495–499.

[17] J. Costamagna, G. Ferraudi, B. Matsuhiro, M.C. Vallette, J. Canales, M. Villagra'n, J. Vargas, M.J. Aguirre, Coord. Chem. Rev. 196 (2000) 125–164.

[18] G. Nirmala, A. Kalilur Rahiman, S. Sreedaran, R. Jegadeesh, N. Raaman, V. Narayanan, Spectrochim. Acta A 77 (2010) 92–100.

[19] C.N. Verani, E. Rentschler, T. Weyhermuller, E. Bill, P. Chaudhuri, J. Chem. Soc., Dalton Trans. (2000) 251–258.

[20] I. Ahmad, A.J. Beg, J. Ethnopharmacol. 74 (2001) 113–123.

[21] J.M. Andrews, J. Antimicrob. Chemother. 48 (2001) 5–16.

[22] J. Marmur, J. Mol. Bio. 3 (1961) 208–218.

[23] H. Chao, W. Mei, Q. Huang, L. Ji, J. Inorg. Biochem. 92 (2002) 165–170.

[24] M. Lee, A.L. Rhodes, M.D. Wyatt, S. Forrow, J.A. Hartley, Biochemistry 32 (1993) 4237–4245.

[25] P. Sathyadevi, P. Krishnamoorthy, E. Jayanthi, R. Butorac, A.H. Cowley, N. Dharmaraj, Inorg. Chim. Acta 384 (2012) 83–96.

[26] T. Mosmann, J. Immuno. Method 65 (1983) 55–63.

[27] R.M. Silverstein, G.C. Bassler, T.C. Morrill, Spectrometric Identification of Organic Compounds. Fifth Edition, John Wiley & Sons, 1991.

[28] K. Shanmuga Bharathi, S. Sreedaran, A. Kalilur Rahiman, V. Narayanan Spectrochim. Acta A 105 (2013) 245–250.

[29] M. Qian, S. Gou, S. Chantrapromma, S. Shanmuga Sundara Raj, H.K. Fun, Q. Zeng, Z. Yu, X. You, Inorg. Chim. Acta 305 (2000) 83–90.

[30] W.B. Tolman, R.L. Rardin, S.J. Lippard, J. Am. Chem. Soc. 11 (1989) 4532–4538.

[31] M. Thirumavalavan, P. Akilan, M. Kandaswamy, Inorg. Chem. 42 (2003) 3308–3317.

[32] W.J. Geary. Coord. Chem. Rev. 7 (1971) 81–122.

[33] G.K. Bareford, G.M. Freeman, D.G. Erver, Inorg. Chem. 86 (1986) 552–558.

[34] W. Levinson & E. Jawetz (1996). Medical microbiology and immunology, 4th Ed. Stanford.

[35] Z. H. Chohan, A. Scozzafova, C. T. Supuran, J. Enzyme Inhib. Med. Chem. 18 (2003) 259–263.

[36] X. Qiao, Z.Y. Ma, C.Z. Xie, Y.W. Zhang, J.Y. Xu, Z.Y. Qiang, J.S. Lou, G.J. Chen, S. Pyan, J. Inorg. Biochem. 105 (2011) 728–737.

[37] J.K. Barton, A.T. Danishefsky, J.M. Goldberg, J. Am. Chem. Soc. 106 (1984) 2172–2176.

[38] A. Kamath, K. Naik, S.P. Netalkar, D.G. Kokare, V.K. Revankar, Med. Chem. Res. 22 (2013) 1948–1956.

[39] J. Qing, W. Gu, H. Liu, F.X. Gao, L. Feng, S.P. Yan, D.Z. Liao, P. Cheng, Dalton Trans. 10 (2007) 1060–1066.

[40] J.W. Mao, H. Zhou, Y.F. Chen, G.Z. Cheng, Z.Q. Pan, Transition Met. Chem 37 (2012) 385–391.

[41] J.-B. Lepecq, C. Paoletti, J. Mol. Biol. 27 (1967) 87–106.

[42] D.L. Boger, B.E. Fink, S.R. Brunette, W.C. Tse, M.P. Hedrick, J. Am. Chem. Soc. 123 (2001) 5878–5891.

[43] M.T. Carter, M. Rodriguez, A.J. Bard, J. Am. Chem. Soc. 111 (1989) 8901–8911.

[44] J.M. Kelly, E.G. Lyons, J.M.V. Putten, R.E. SmythM, in: Analytical chemistry, symposium series, Electrochemistry, Sensors and Analysis [M], Vol. 25, Elsevier, Amsterdam, 1986, p. 205.

[45] G. Prativel, M. Pitie, J. Benadou, B. Meunier, Angew. Chem. Int. Ed. Eng. 30 (1991) 702–704.

[46] B.K. Keppler, B.K. Holler, 'Metal complexes in cancer chemotherapy', VCH, Weinheim (1993) 37.

[47] C. Negri, R. Berhardi, A. Braghetti, G.C. Ricotti, A.L. Scovassi, Carcinogenesis 14 (1993) 2559–2564.

[48] Y.A. Lazebnik, S.H. Kawfmann, S. Desnoyers, G.G. Poirier, W.C. Earnshaw, Nature 371 (1994) 364–347.

[49] M. Tewari, L.T. Quan, K. O'Rourke, S. Desnoyers, Z. Zeng, D.R. Beidler, G.G. Poirier, G.S. Salvesen, V.M. Dixit, Cell 81 (1995) 801–809.

[50] P. Jaividhya, R. Dhivya, M.A. Akbarsha, M. Palaniandavar, J. Inorg. Biochem. 114 (2012) 94–105.

[51] N.P. Singh, M.T. McCoy, R.R. Tice, E.L. Schneider, Exp. Cell. Res 175 (1988) 184–191.

FIGURE CAPTIONS:

Scheme 1.

Schematic route for synthesis of ligands.

Scheme 2.

Cyclocondensation of 2,6-diformyl-4-methylphenol and various diamines with nickel(II) and copper(II) perchlorates as metal template.

Fig. 1.

^{1}H NMR spectra of ligands L (a), L' (b) and L" (c).

Fig. 2.

High resolution masss spectrum [HRMS] of 2,2'-3,5-dinitrobenzoylimino di(ethylamine) trihydrochloride (L").

Fig. 3.

ESI mass spectrum of complex **3**.

Fig. 4.

Absorption spectra of complexes **2** (a) and **3** (b) in Tris-HCl/NaCl buffer at pH 7.2 upon addition of CT-DNA, [Complex] = 100 µM, [DNA] = (0–100 µM). Arrow shows the absorbance change upon increase of DNA concentration. Inset: Plot of [DNA]/($\varepsilon_a - \varepsilon_f$) *vs* [DNA] for the titration of DNA with complexes **2** and **3**.

Fig. 5.

Absorption spectra of complexes **5** (a) and **6** (b) in Tris-HCl/NaCl buffer at pH 7.2 upon addition of CT-DNA, [Complex] = 100 µM, [DNA] = (0–100 µM). Arrow shows the absorbance change upon increase of DNA concentration. Inset: Plot of [DNA]/($\varepsilon_a - \varepsilon_f$) *vs* [DNA] for the titration of DNA with complexes **5** and **6**.

Fig. 6.

Emission spectra of complexes **2** (a) and **3** (b), in Tris-HCl/NaCl buffer at pH 7.2 in the absence and presence of CT-DNA, [Complex] = (0–100 µM), [DNA] = 10 µM. Arrow shows the fluorescence changes upon increasing DNA concentration. Inset: Plots of emission intensity I_0/I *vs* [DNA]/[Complex] for the titration of complexes **2** and **3**.

Fig. 7.

Emission spectra of complexes **5** (a) and **6** (b) in Tris-HCl/NaCl buffer at pH 7.2 in the absence and presence of CT-DNA, [Complex] = (0–100 μM), [DNA] = 10 μM. Arrow shows the fluorescence changes upon increasing DNA concentration. Inset: Plots of emission intensity I_0/I *vs* [DNA]/[Complex] for the titration of complexes **5** and **6**.

Fig. 8.

Cyclic voltammograms of complexes **2** (a), **3** (b), **5** (c) and **6** (d) in DMF-Tris-HCl/NaCl buffer at pH 7.2 in the absence (solid line) and presence (dotted line) of CT-DNA and arrow mark indicates the current changes upon increasing DNA concentration.

Fig. 9.

Changes in the agarose gel electrophoretic pattern of CT-DNA induced by H_2O_2 and metal complexes: Lane 1: DNA alone; Lane 2: DNA + **1** + H_2O_2; Lane 3: DNA + **5** + H_2O_2; Lane 4: DNA + **4** + H_2O_2; Lane 5: DNA + **6** + H_2O_2.

Fig. 10.

Dose dependent curves (percentage viability curves) of the HepG2 cell line after treatment with complexes **2** (a), **5** (b) and **6** (c). Viability was checked by MTT assay after 24 h and 48 h.

Fig. 11.

Morphology of control and complexes treated HepG2 liver cancer cell line (40X magnification) control (a) and complexes **2** (b)**, 5** (c) and **6** (d).

Fig. 12.

The morphological changes of PI stained HepG2 cell line after treatment with complexes as observed under a fluorescence microscope. Cells were treated without complex (a) or with complex **2** (b) **5** (c) and **6** (d).

Fig. 13.

Analysis of apoptotic inducing effect of pendant-armed complexes on HepG2 cell line assessed by comet assay. Control (a) and complexes at IC_{50} concentration **2** (b)**, 5** (c) and **6** (d).

Table 1. Antibacterial screening data of complexes

Compounds	Representation zone of inhibition (mm)				
	Gram –ve		Gram +ve		
	P.v	***E.f***	***S.a***	***S.m***	***S.p***
Ciprofloxacin	22	24	25	25	24
1	5	5	-	6	6
2	6	6	8	7	7
3	9	9	8	8	12
4	6	10	8	6	10
5	9	12	10	7	12
6	15	12	18	10	15

Standard: Ciprofloxacin 5 µg/mL; Complxes **1**–**6** each at a concentration of 150 µg/mL.
P.v - Proteus vulgaris; E.f - Enterococcus faecalis; *S.a - Staphylococcus aureus;*
S.m - Streptococcus mutants; *S.p - Streptococcus pneumoniae*

Table 2. DNA-binding constants (k_b), Stern-Volmer quenching constants (k_{sv}) and IC_{50} values of complexes against HepG2 cancer cell line.

Complexes[a]	$K_b \times 10^2$ (M^{-1})	$K_{sv} \times 10^5$ (M^{-1})[b]	IC_{50} (μM)[c]		Percentage of tail DNA
			24 h	48 h	
2	1.13	0.10	8.5	8.9	65.1
3	1.50	0.67	-	-	-
5	6.03	1.05	1.7	2.1	75.5
6	8.50	2.24	1.0	2.0	88.4

[a][Complex] = 10 μM.
[b]Relative emission intensity enhancement in the presence of CT-DNA at [DNA] = 1.0×10^{-5} M, [Complex] = $0–10 \times 10^{-5}$ M.
[c]Cytotoxicity of binuclear complexes **2**, **5** and **6** on HepG2 cells.

Table 3. Electrochemical parameters for complexes 1–4 in the absence and presence of CT-DNA.

Complexes	R	i^1_{pc} (10^{-5}A)	i^2_{pc} (10^{-5}A)	E^1_{pc}	E^2_{pc}
2	0	1.50	1.10	−0.75	−1.25
	1	1.30	1.01	−0.72	−1.21
3	0	1.30	1.02	–0.74	–1.24
	1	1.10	0.80	–0.71	−1.21
5	0	1.41	1.23	–0.76	–1.26
	1	0.72	1.10	–0.70	−1.20
6	0	1.15	1.45	–0.75	–1.23
	1	0.70	1.12	–0.69	–1.22

CV measured at 100 mV^{-1}. E (V) *vs*. Ag/AgCl Conditions: GC working, Pt wire counter and Ag/AgCl reference electrode; R = [DNA]/[Complex]; [DNA] = 200 µM; [Complex] = 100 µM; Supporting electrolyte (TBAP) = 0.1 M.

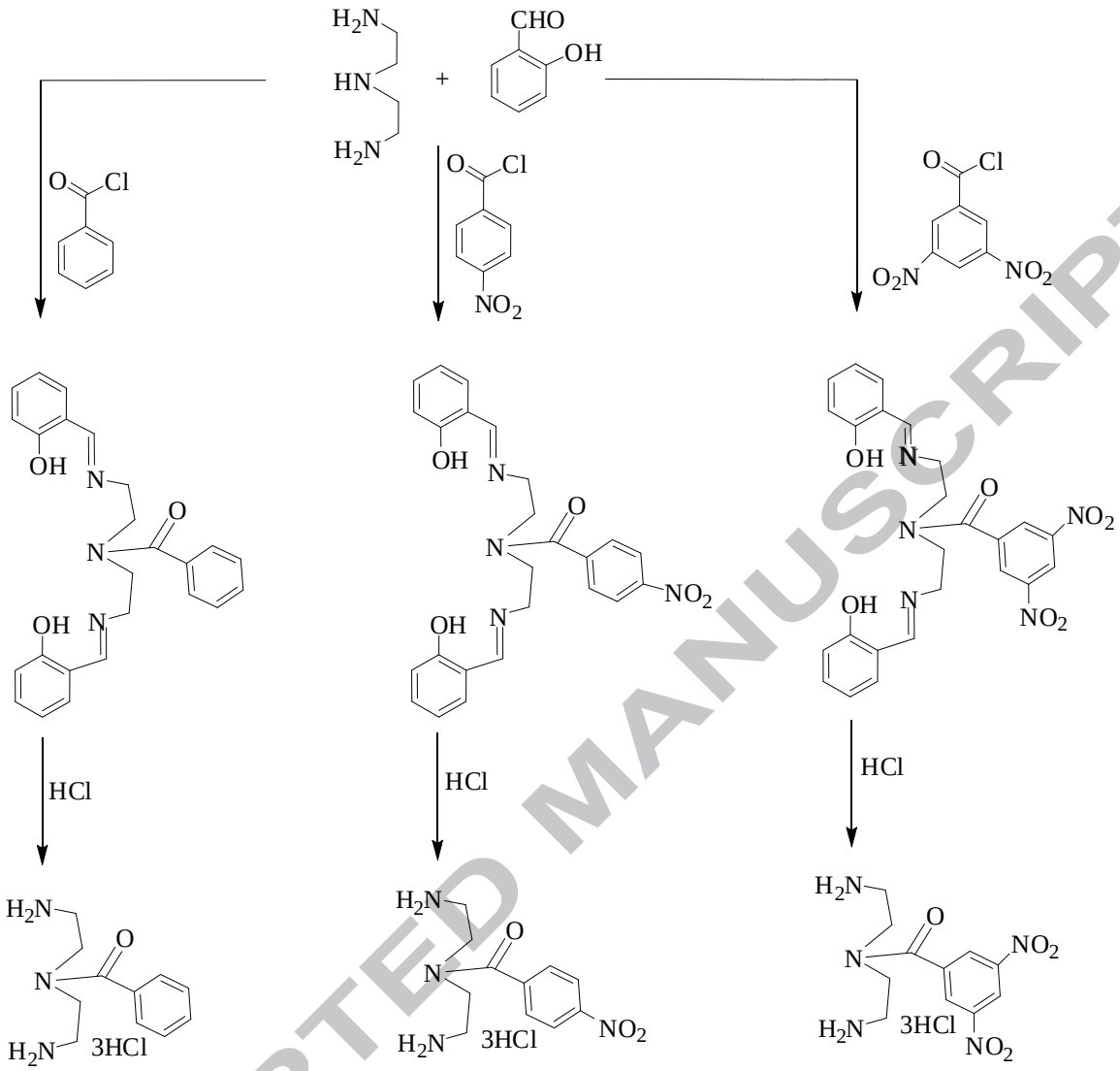

Scheme 1.

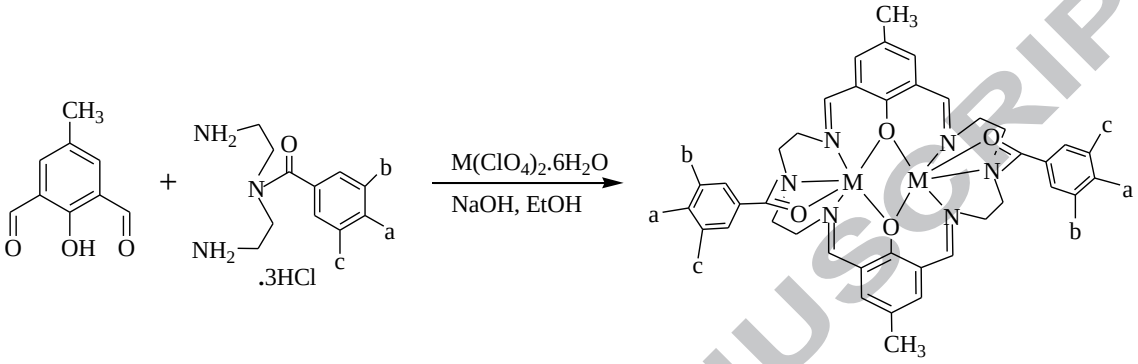

	a	b	c
L^1	H	H	H
L^2	NO_2	H	H
L^3	H	NO_2	NO_2

M = Ni(II) (or) Cu(II)

Scheme 2.

(a)

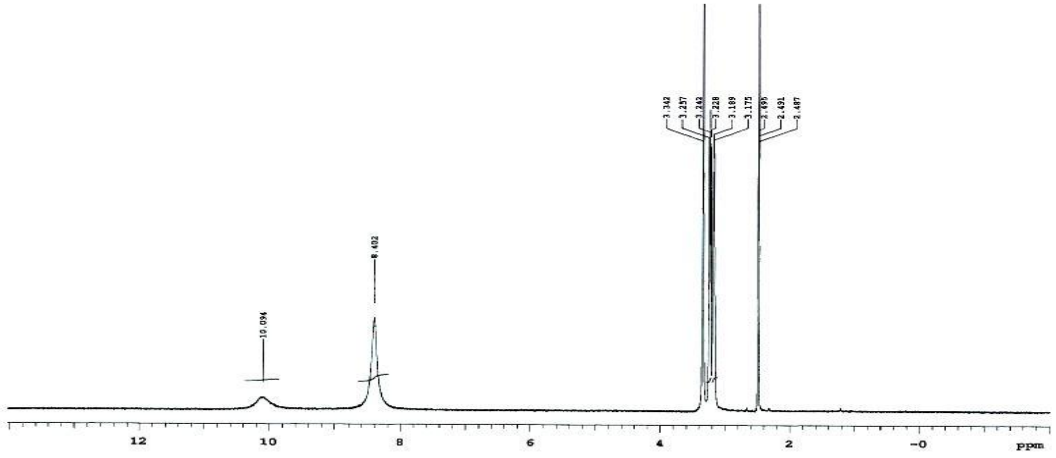

(b)

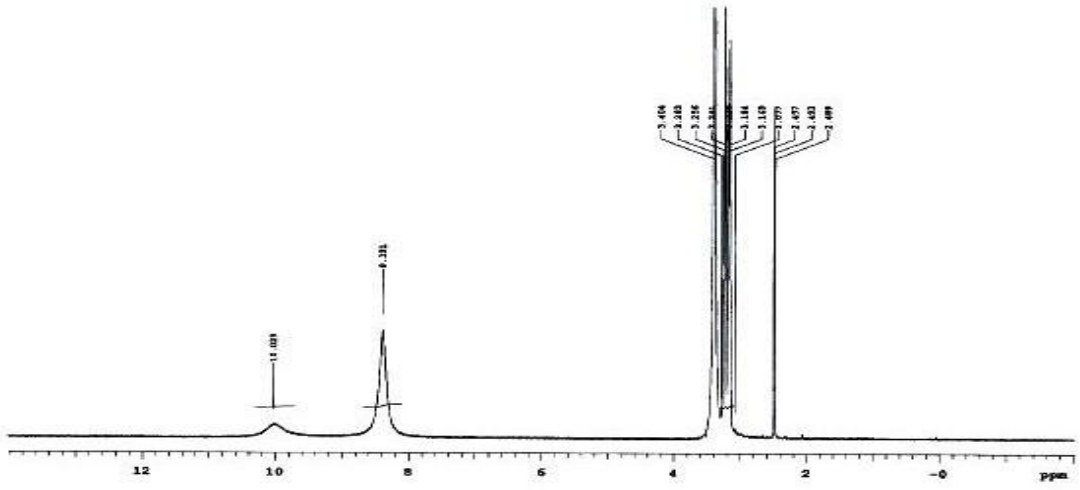

(c)

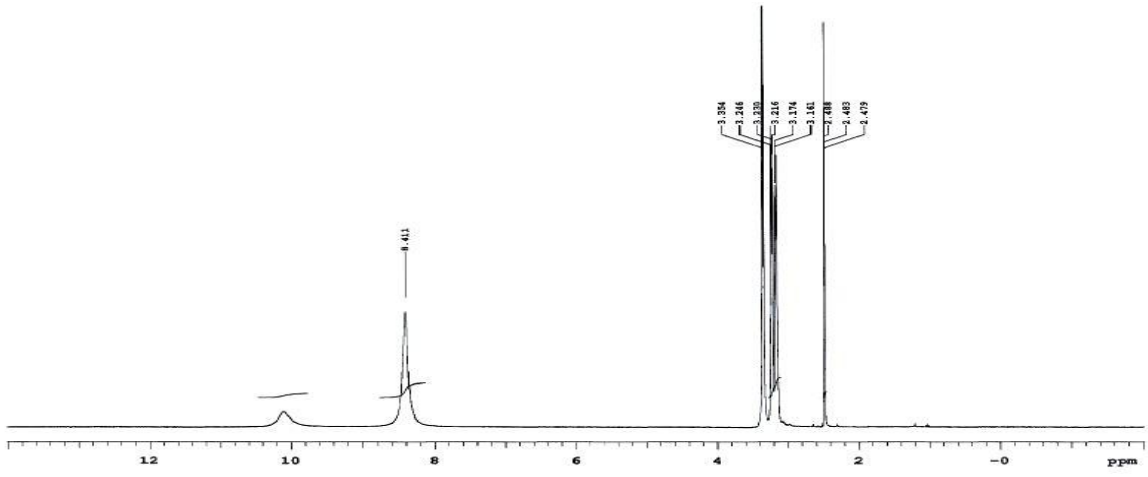

Fig. 1.

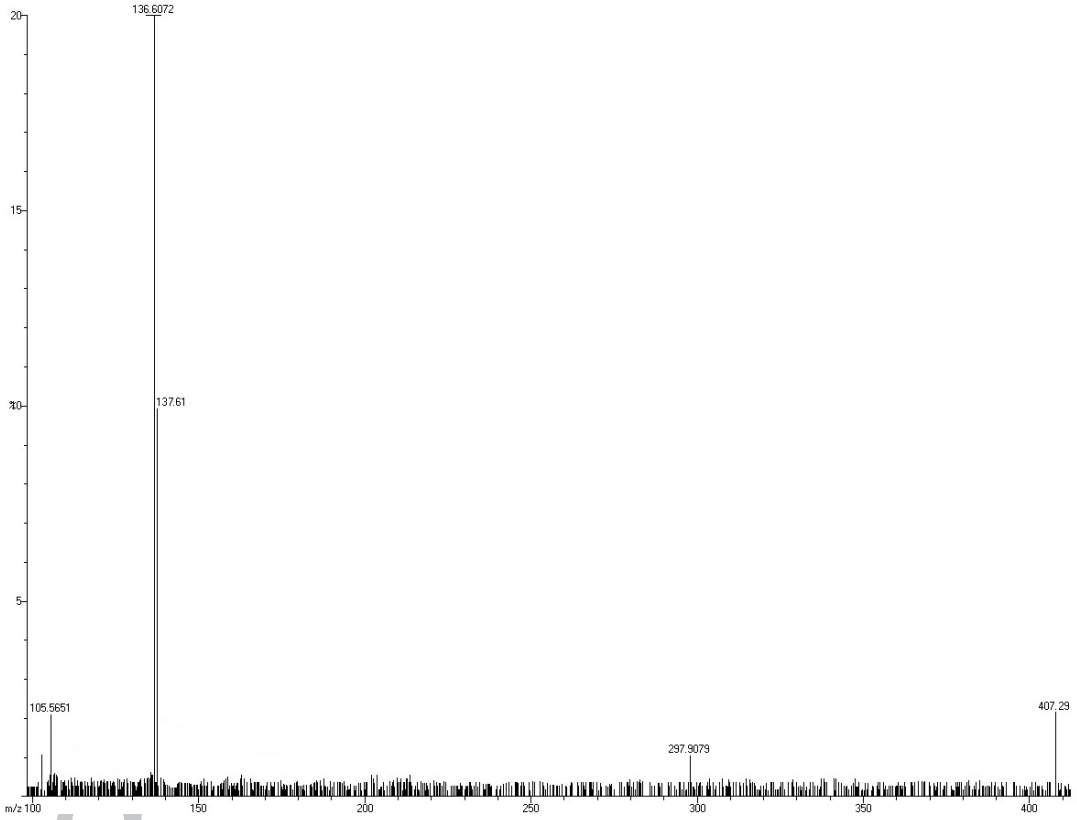

Fig. 2.

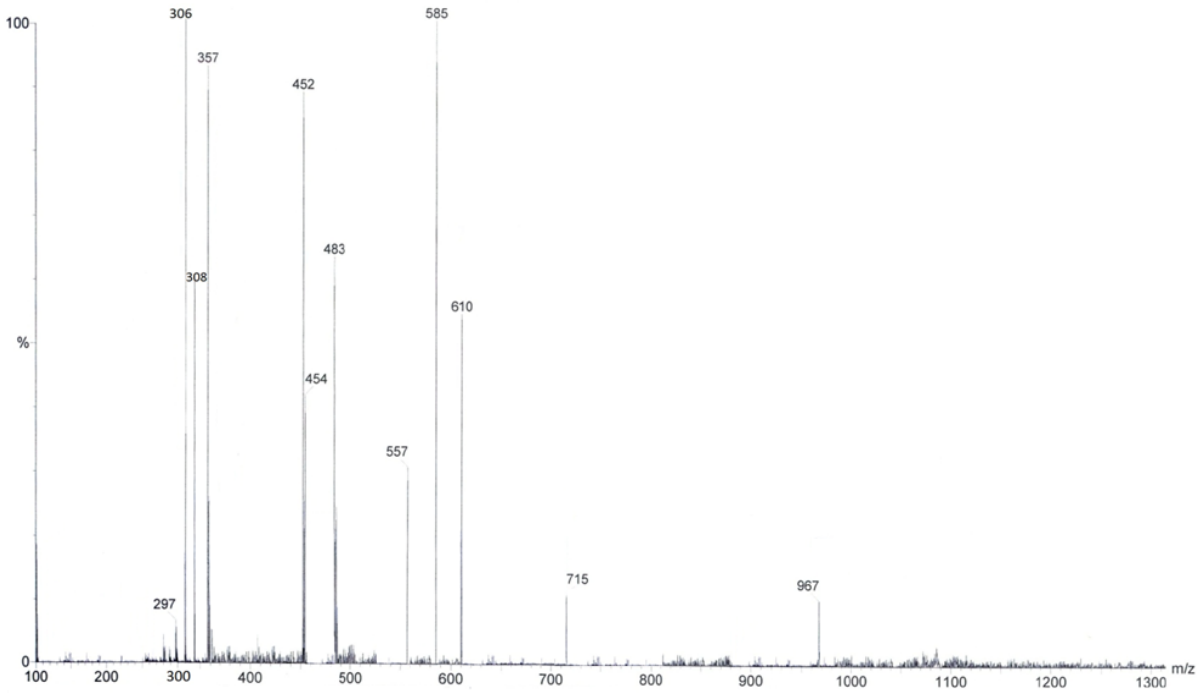

Fig. 3.

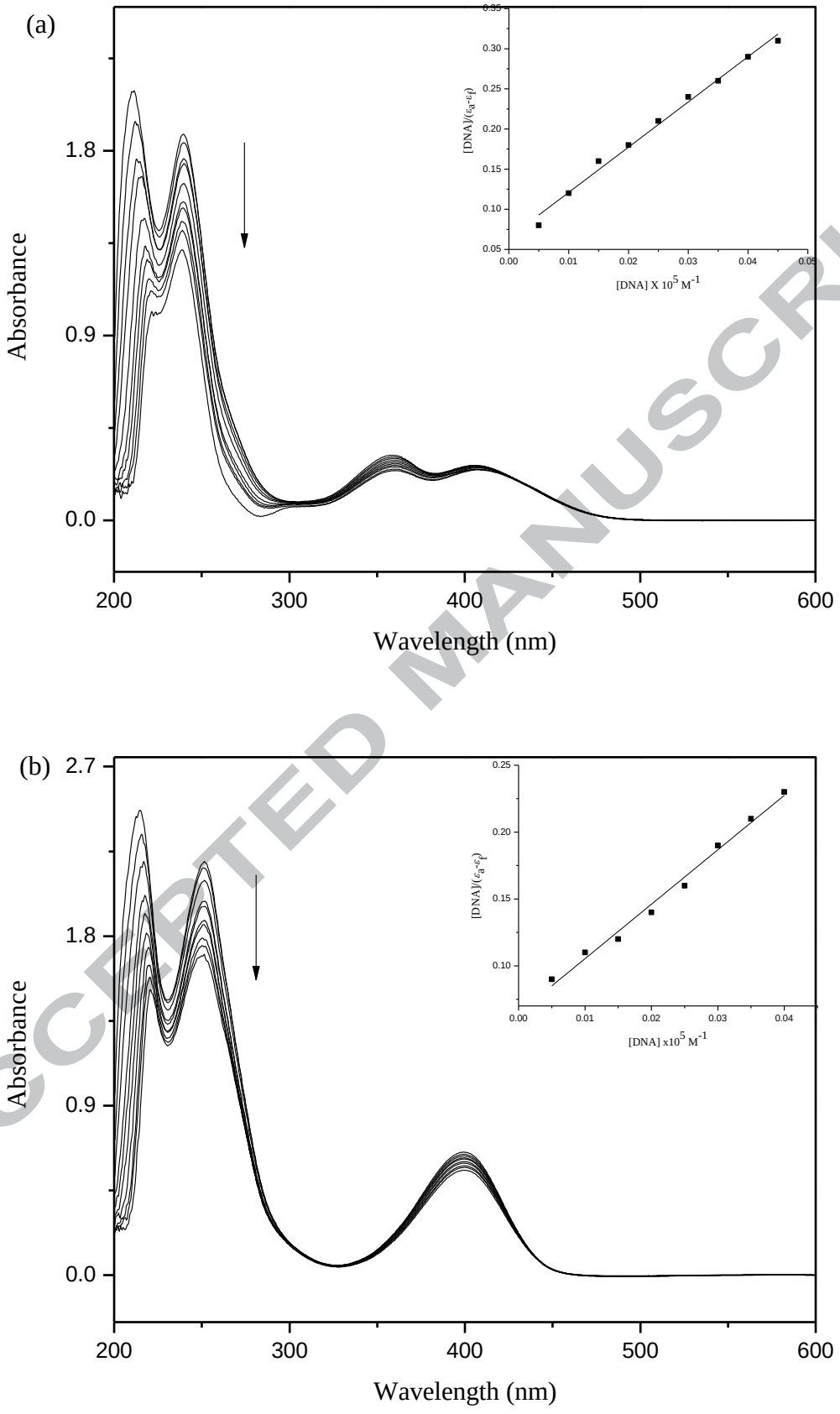

Fig. 4.

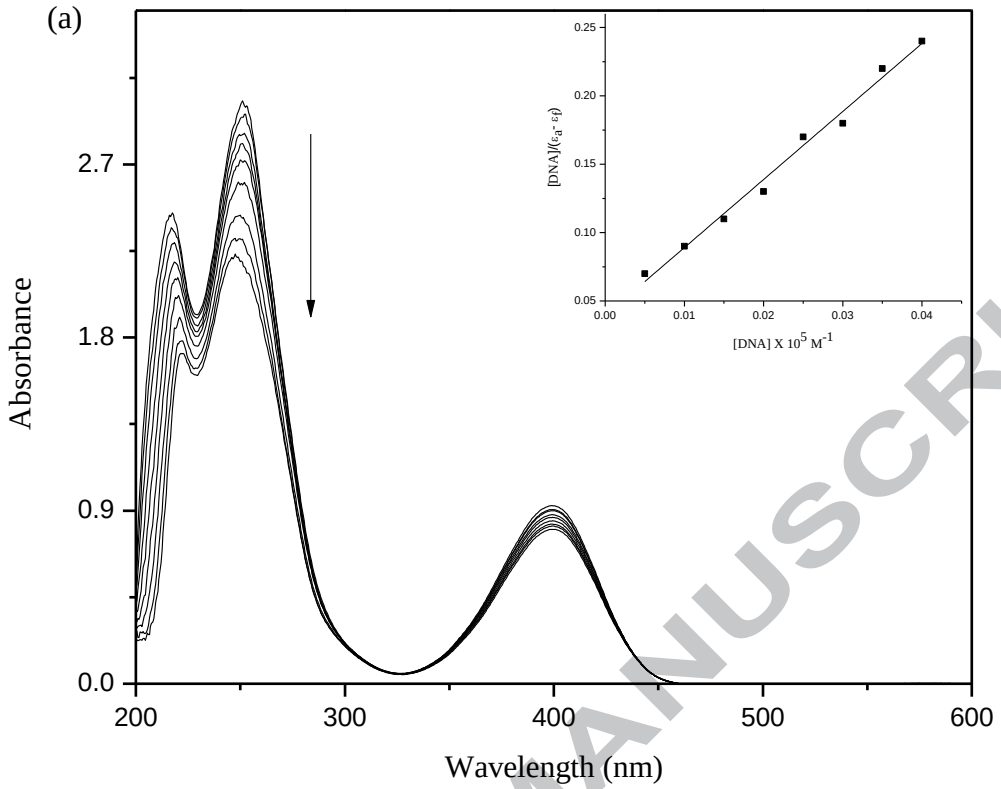

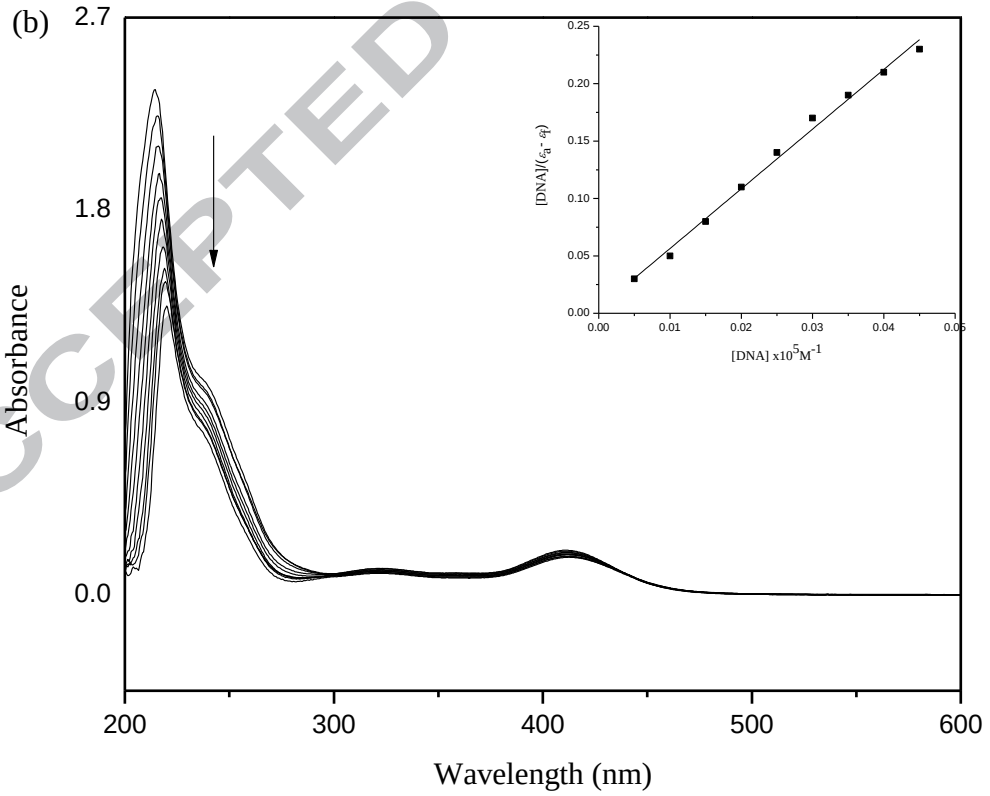

Fig. 5.

(a)

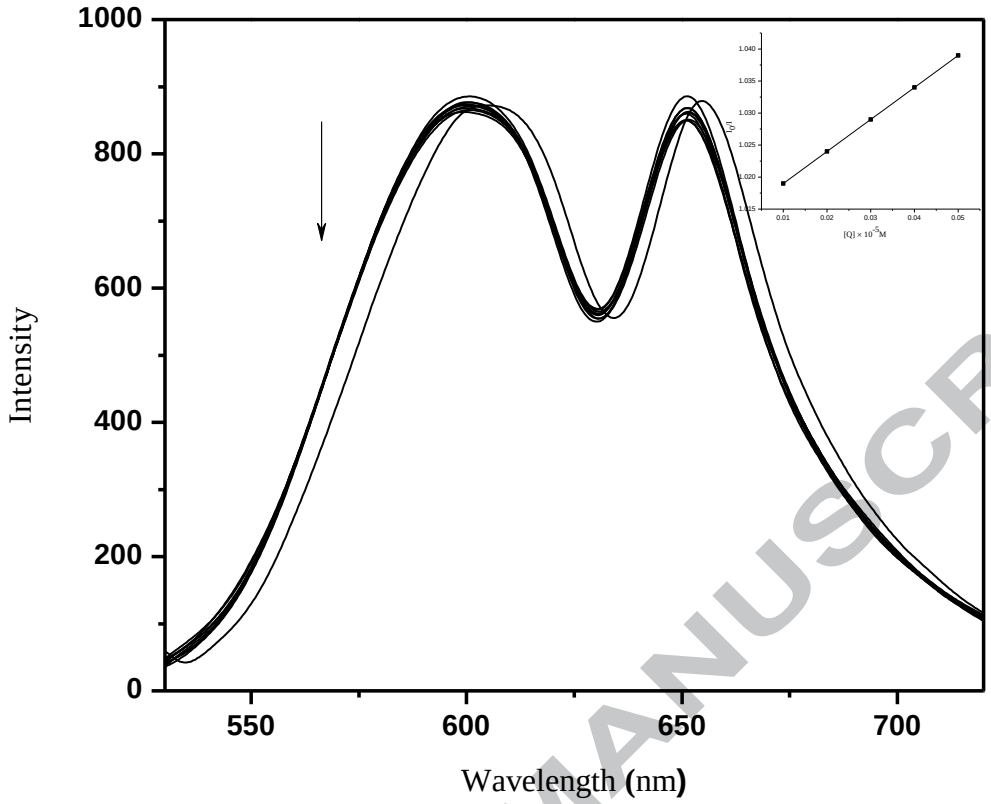

(b)

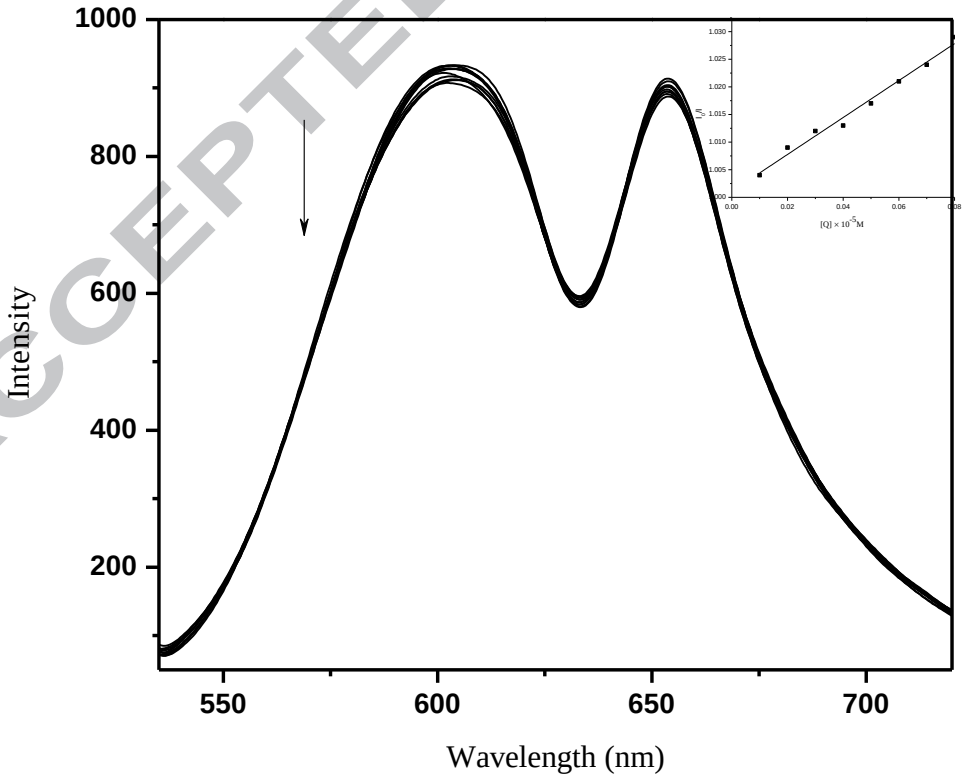

Fig. 6.

(a)

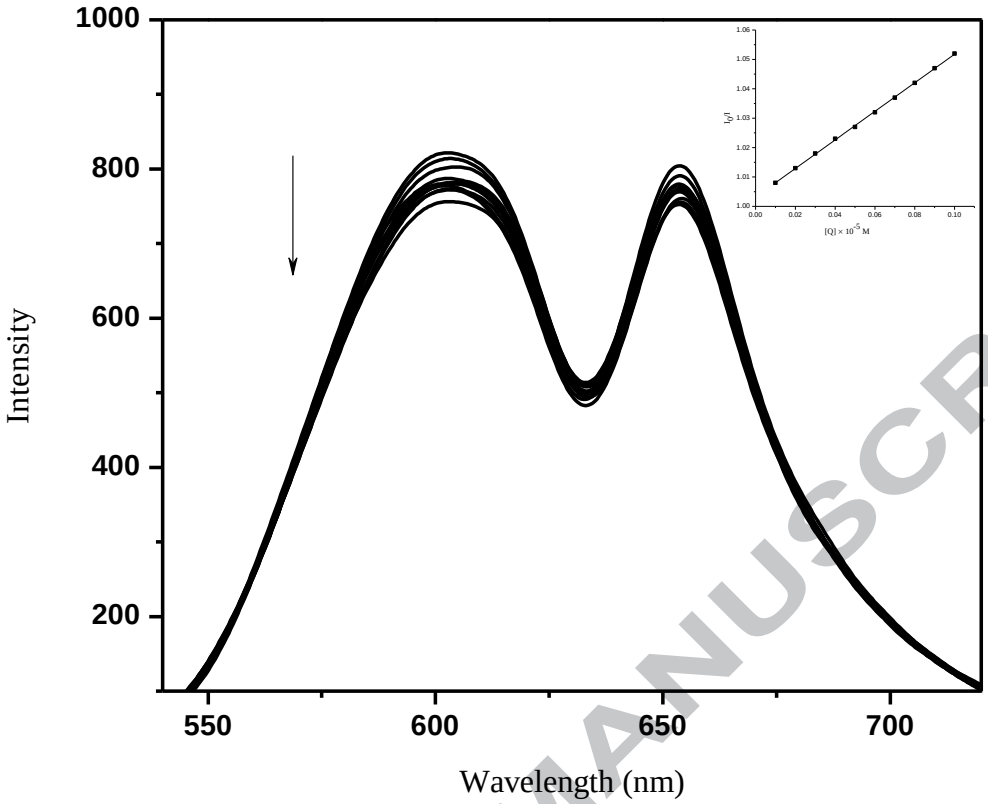

(b)

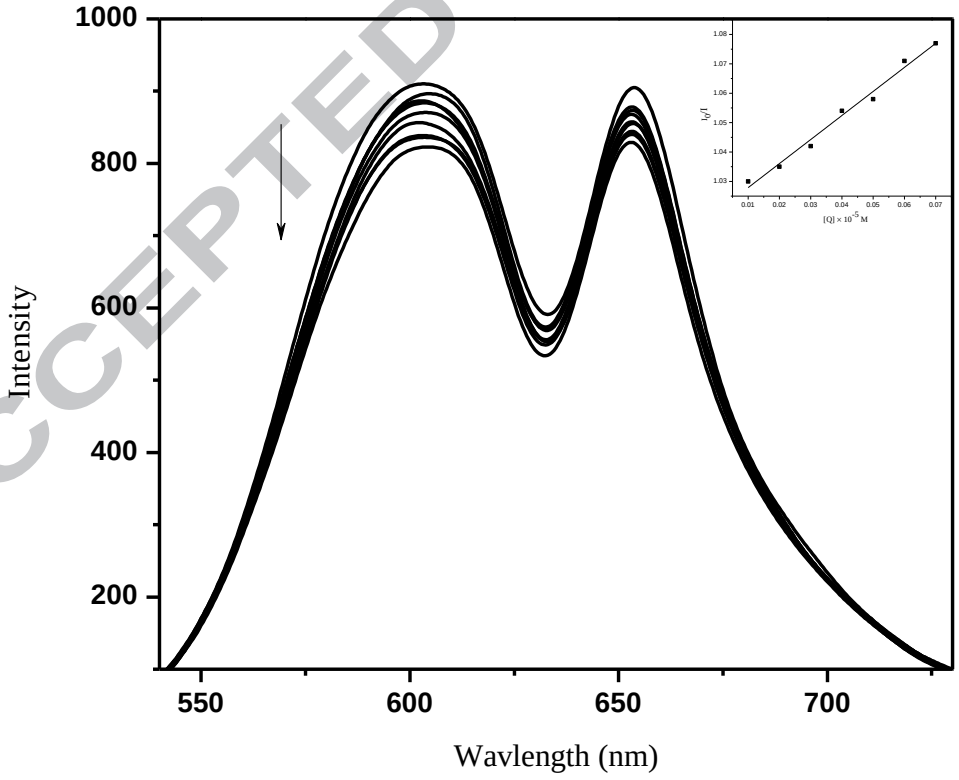

Fig. 7.

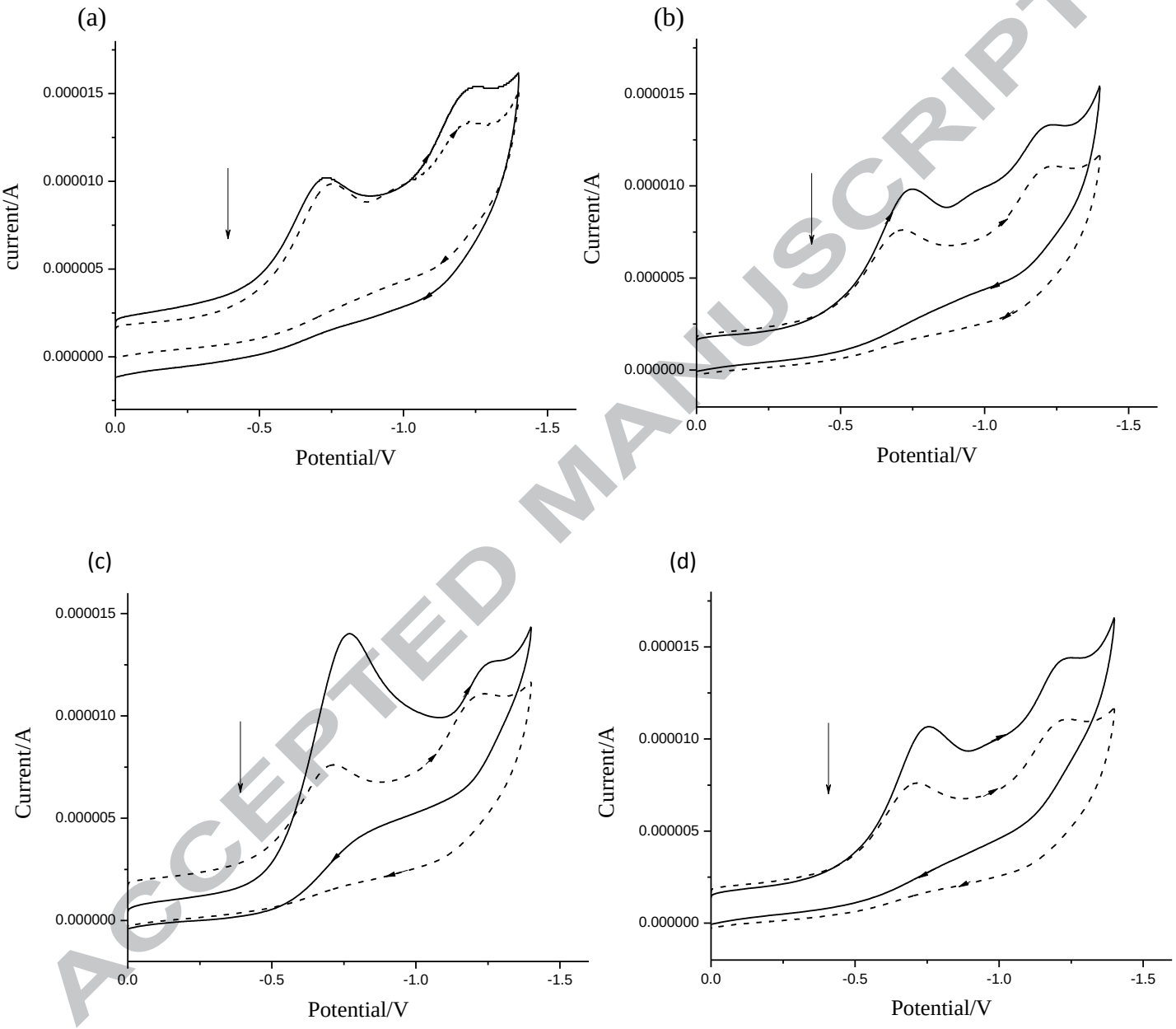

Fig. 8.

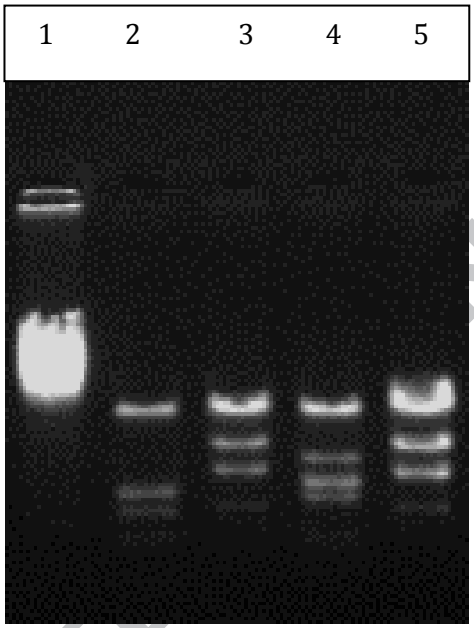

Fig. 9.

(a)

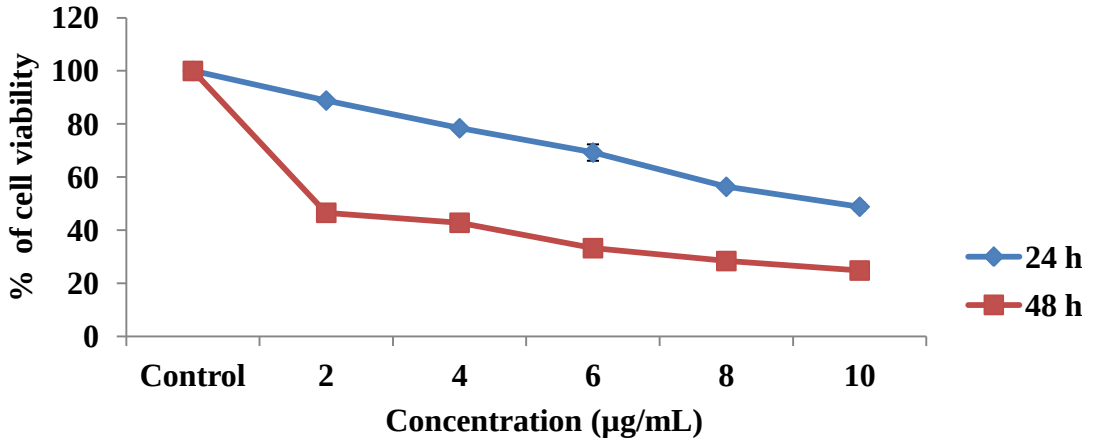

(b)

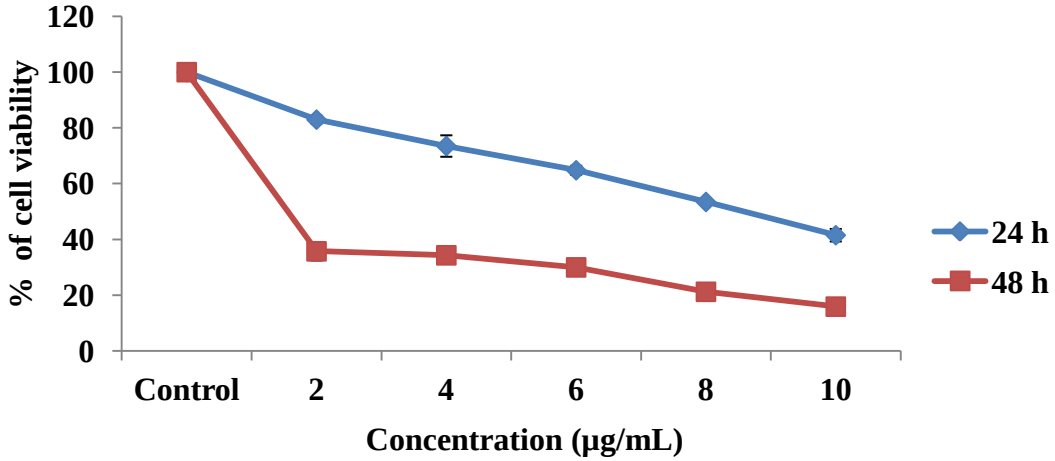

(c)

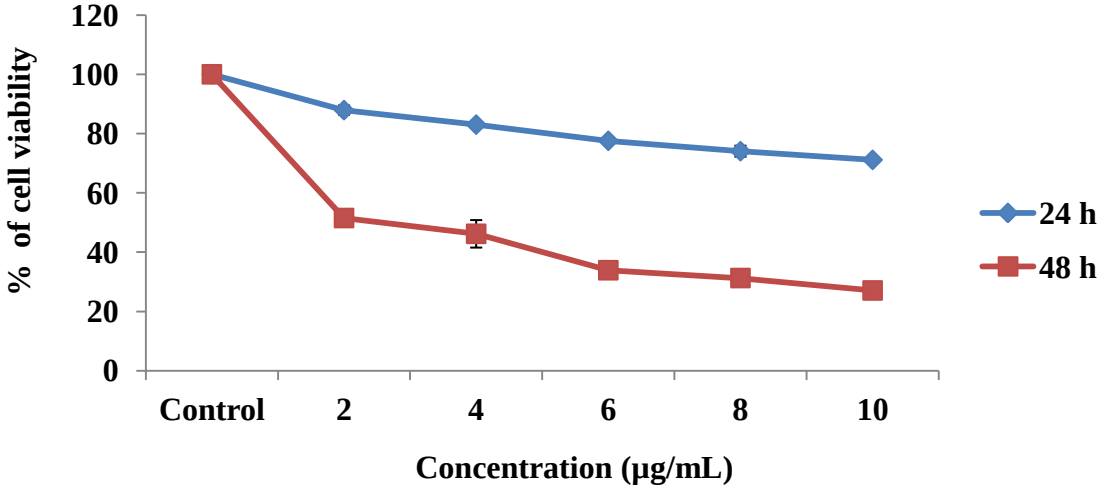

Fig. 10.

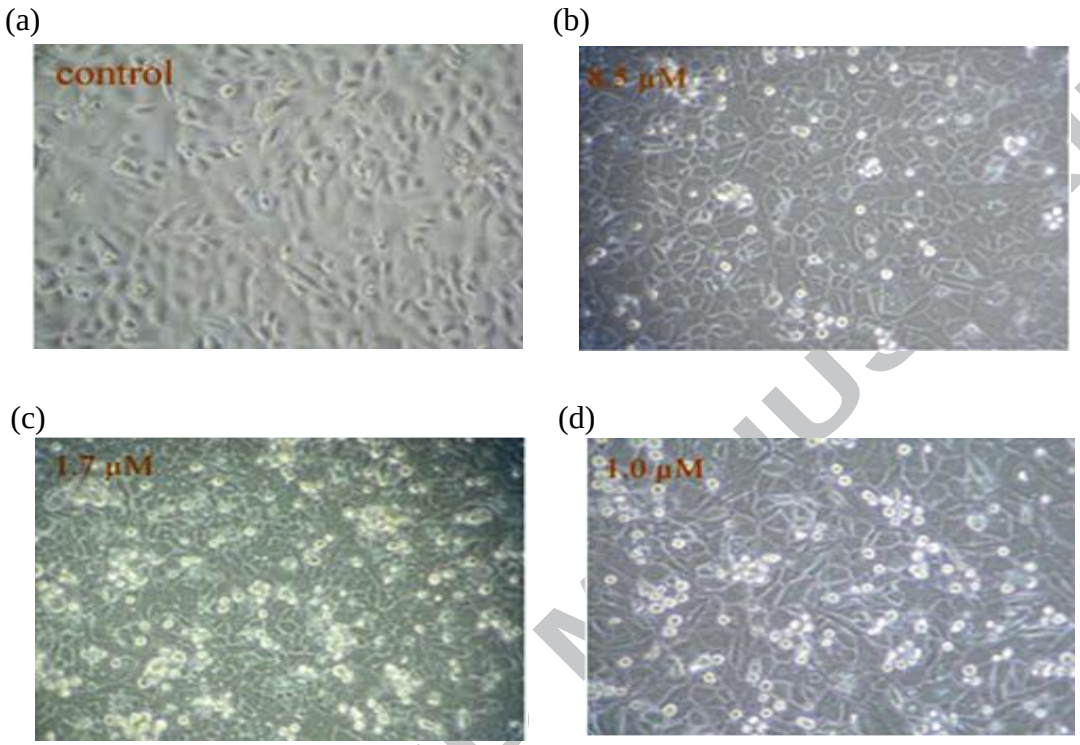

Fig. 11.

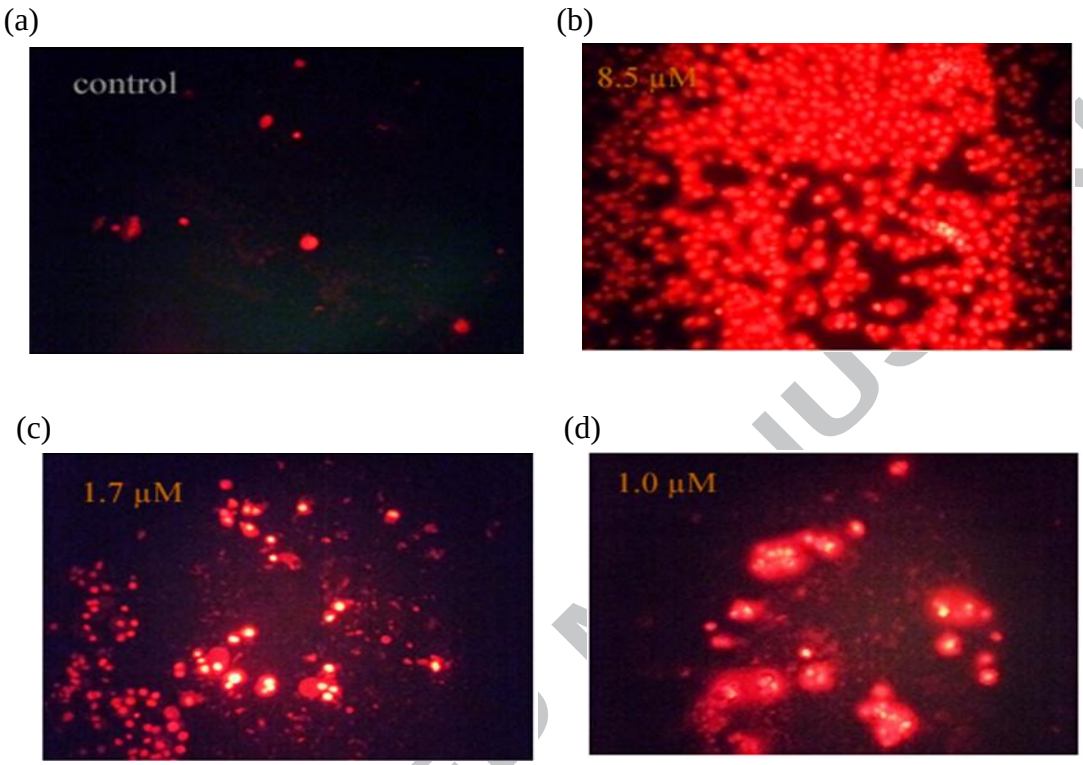

Fig. 12.

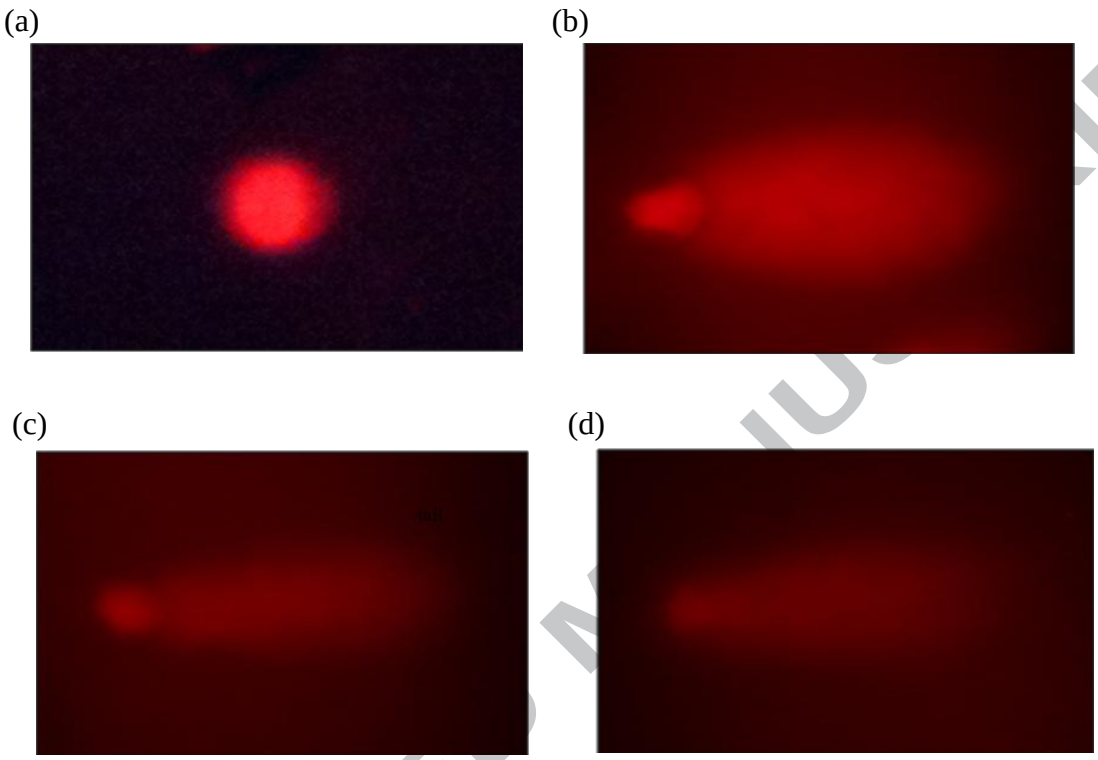

Fig. 13.

HIGHLIGHTS

- Six pendant-armed complexes with benzoyl substituents have been synthesized.
- Antibacterial activity against Gram +ve and Gram –ve bacteria has been studied.
- DNA binding studies suggest the intercalative mode of binding.
- The synthesized complexes act as potent metallonucleases.
- Complexes can enter the nuclei of HepG2 cells and induce cell apoptosis.

ANTIBACTERIAL, DNA INTERACTION AND CYTOTOXIC ACTIVITIES OF PENDANT-ARMED POLYAMINE MACROCYCLIC DINUCLEAR NICKEL(II) AND COPPER(II) COMPLEXES

P. Arthi[a], A. Haleel[a], P. Srinivasan[b], D. Prabhu[c], C. Arulvasu[c], A. Kalilur Rahiman[a,*]

[a]*Post-Graduate and Research Department of Chemistry, The New College (Autonomous), Chennai-600 014, India*

[b]*Department of Bioinformatics, Alagappa University, Karaikudi-630 003, India*

[c]*Department of Zoology, University of Madras, Guindy Maraimalai Campus, Chennai-600 025, India*

Graphical Abstract